EXPERIMENTS DIVISION

Doc. Nr.	EDMS	Created	Printed	Pages	Revision
EXD-BL04-GD-0001		2007-02-08	2007-02-13	42	3

Conceptual Design Report of the Materials Science and Powder diffraction beam line MSPD at ALBA

ABSTRACT

This document describes the design concept of the MSPD beam line at the new 3rd generation synchrotron source ALBA near Barcelona/Spain. It considers mainly the optics of the beam line. Design variants as well as the preferred solution for different elements are given and briefly discussed. Some background technical information is provided to give the opportunity to evaluate the presented or alternative solutions.

Prepared by	Checked by	Approved by
Michael Knapp and Inma Peral	K. Klementiev J. Juanhuix	S. Ferrer

Distribution list

Contents

1 Beam line scientific scope

The Spanish user community proposed a beam line capable of performing i) high resolution and in-situ powder diffraction, ii) single crystal, and iii) high pressure diffraction on powders and single crystals. To comply this, the beam line should be able to operate from 8keV to 50keV. This energy range will cover most of the needs for the materials science community. In particular the high energy region (30-50keV) provides an optimum energy range for high pressure experiments and is also desirable for high resolution powder diffraction experiments. The detailed scientific case can be obtained from the original beam line proposal (see section 9 for reference).

Accordingly, the energy range has determined the type of source (a superconducting wiggler), and the implemented techniques the number of experimental stations (2). Finally, the optics has been designed to accommodate the source and the two experimental stations. It has always been kept in mind that the optical design should be compact, and that all components must easily be changeable without major realignments. Considering the different optical requirements for the two end stations, a modular concept has been chosen, where it's in principle possible to combine the basic arrangement with additional optical elements. Taking all of this into account, the MSPD BL has been designed to facilitate diffraction experiments in the hard x-ray regime between 8 and 50keV with the main operational region between 30-50keV. The first end-station is dedicated to single-crystal diffraction and diffraction at high pressures generated by diamond anvil cells. The second one for diffraction on polycrystalline samples (powder diffraction).

1.1 Experimental stations and techniques

Station 1:

SC: Single crystal small molecule diffraction,
Electron density mapping,
HP: High pressure diffraction on powders and
single crystals with diamond anvil cells (DAC)
and laser heating as a near future option.

Station 2:

PD: Powder diffraction, High resolution powder diffraction,
in-situ at non ambient conditions, and total scattering experiments

1.2 Energy range, energy resolution and beam properties at the experimental stations

Energy range:

Maximum: 8-50keV (1.5 - 0.25Å)
Typical: 20-40keV (0.6 - 0.3Å)
(Lower energies are accessible under reduced performance)

Energy resolution: $2 \cdot 10^{-4}$ dE/E

Beam divergence: Expected divergences are given in section 4.

Typical beam sizes (H x V):   HRPD: 5 x 2 mm^2

SC: 0.3 x 0.3 mm^2

HP: 0.05 x 0.05 mm^2

HP + laser heating: 30 x 20 μm^2

The typical beam size in powder diffraction is about 1.5x5mm^2 while the typical size in single crystal diffraction is of 0.3 x 0.3mm^2 or even smaller (50 x 50μm^2) for high pressure powder diffraction. For moderate sizes (down to 50μm) the beam will be shaped by slits and collimators. However, for high pressure diffraction above 20GPa and when using laser heating beam sizes of the order or 20μm or less are needed. As focusing optics a KB-mirror for station 1 is proposed.

A sagittally curved mirror downstream the monochromator partially focuses the beam in the horizontal plane for the PD station. This mirror also has a meridional bender to focus in the vertical plane. By slightly increasing the mirrors glancing angle it's possible to focus on station 1 up to energies of 26keV.

2   The source

The high energy regime is reached with a superconducting wiggler with short period length and variable K-value. Generated flux/power and divergences depend on the K-value and the storage ring current. The IDs K value can be varied by changing the coil current of the ID, besides, the nominal current of the storage ring is planned to be 250mA with the option to run at 400mA in the future. Therefore, calculations based on those parameters have been performed; two values of 100% and 60% K_{Max} for high and low energy applications are used in the calculations. The optimization was done by J., Campmany (ALBA) and is described in detail in [Campmany06, 07].

Since the maximum power generated by the ID can reach up to 20kW (maximum synchrotron current at maximum K value), total heat load and power density on all elements in the beam path is an important issue.

Despite the rather low K-value of the device the behavior in the high energy range is very wiggler like even without randomization of the period length. Figure 2.1 gives the flux (on axis) in the interesting energy region for three cases:

- Wiggler with perfect sinusoidal field in the centre.

- Wiggler with field in the centre produced by an arrangement of alternated coils of the same length / perfect periodicity (calculated with RADIA [Chubar98]).

- Wiggler with field in the centre produced by an arrangement of alternated coils with randomized period length (calculated with RADIA). The dispersion of period lengths follows a Gaussian distribution with σ = 1.5μm.
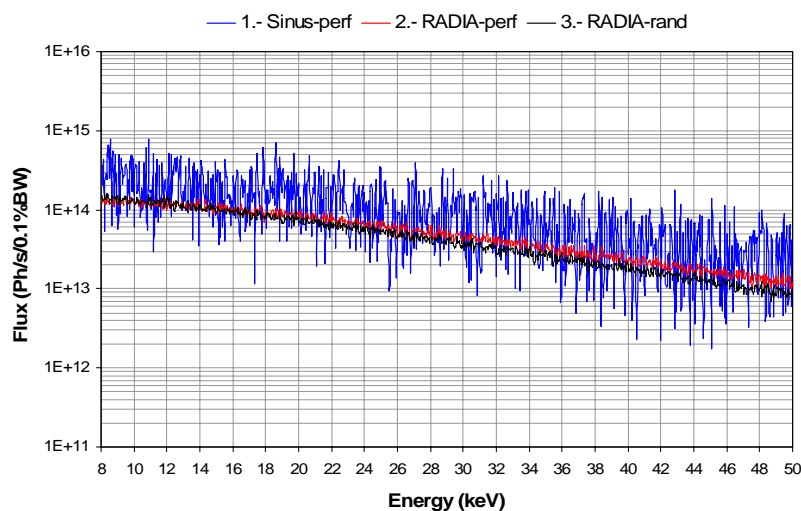
Figure 2.1: Calculated flux in the high energy range for cases given in the text.

As main results we can state:

- Ripple in the case of perfect sinusoidal field: ~57% on average, 363% maximum amplitude

- Ripple in the case of a realistic field calculated with RADIA and perfect periodicity: ~7% on average, 36% maximum amplitude

- Ripple in the case of a realistic field calculated with RADIA and period randomization of 1.5 microns: ~7% on average, 30% maximum amplitude.

The presented results are worst case scenarios, since the spectrum is further smeared out by electron dispersion effects. Additional randomization of the period length is not necessary.

Location in the ring: medium straight section (length: 4 m), BL4/PD

Electron beam in the center of the medium straight section:

σ_x 131.2µm

σ_y 7.4µm

σ_x'   46.3µrad

σ_y'   5.75µrad

Photon beam generated by the ID (calculated with Spectra, K = 6.08, 1ˢᵗ harmonic, zero emittance)

Σ_x: 273µm Σ_x': 500µrad

Σ_y: 55µm Σ_y': 102µrad

FWHM values: (factor 2.354)

X: 643µm   Xp: 1177µrad

Y: 129µm   Yp: 240µrad

ID type: superconducting wiggler SCW31

Total length	2m
Vacuum chamber vertical aperture	8mm
Period length	31mm
Magnetic gap	12.4mm
Number of periods	60.5
Nominal peak field on axis:	2.1T
Maximum K value (variable)	6.08
Maximum total Power	20kW
Power density	47.5kW/mrad^2
Critical Energy @ K_{max}	12.5keV
Electron beam current	250mA / 400mA

ID @ 60%, 400mA:

K	3.65
Nominal peak field on axis	1.26T
E_c	7.5keV
P_{tot}	6.8kW

Beam size and divergence:
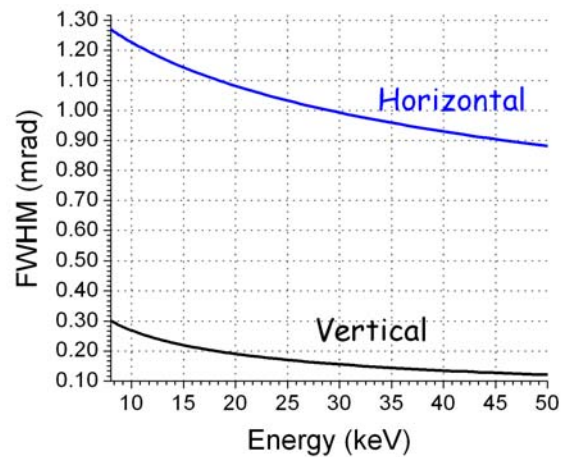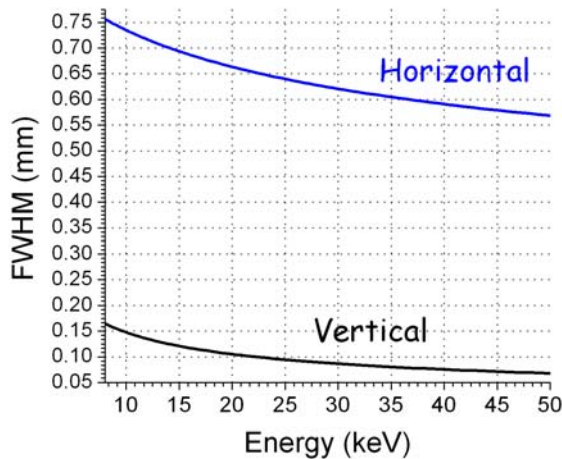
Figure 2.1 FWHM values of the photon beam calculated with Spectra @ K=6.08 (σ x 2.354). The horizontal divergence is not really Gaussian and therefore underestimated in the plot.
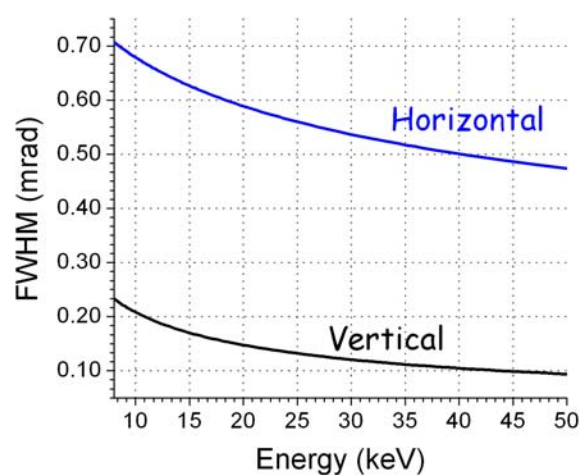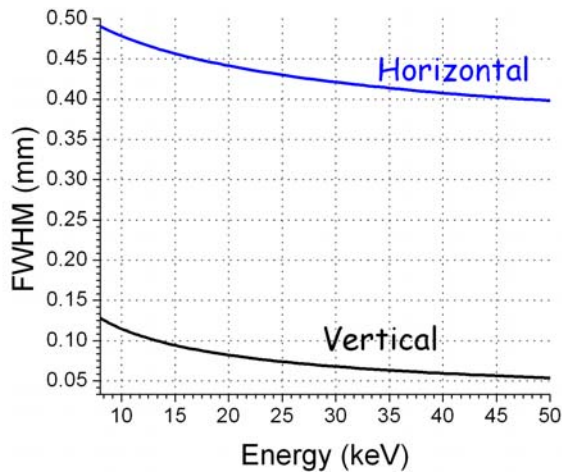
Figure 2.2: FWHM values (size, divergence) calculated with Spectra @ K=3.65 (σ x 2.354). The horizontal divergence is not really Gaussian and therefore underestimated in the plot.

3   Optical layout

3.1   Main optical components scope

Filters

The optical elements are preceded by a variable white beam filter to strip off the low energy part of the wiggler spectrum and reduce the heat load on the downstream optics.

First mirror M1

The first mirror M1 will be installed to i) reduce the heat load on the monochromator ii) suppress higher harmonics and iii) collimate the beam in the vertical direction, thus increasing the energy resolution. This is necessary in order to achieve high resolution powder diffraction data.

Monochromator

The monochromator will produce a monochromatic beam with dE/E of about $2 \cdot 10^{-4}$ in the 8 – 50keV range. The crystals receive high heat load, thus adequate cooling must be provided.

Second mirror M2

The second mirror is used for partial horizontal focusing at station 2, PD, and focusing on station 1, SC/HP, in horizontal and (with a bender) vertical direction.

Focusing KB system with Multilayers

The KB system provides focusing on station 1, SC/HP, for energies > 20keV. Multilayers offer a wide variety in beam conditioning up to 80keV. They can, for instance, be made with either lateral or in-depth grading (super-mirrors) and double layer spacing of 2nm. With super mirrors focusing at different energies without realigning the mirror is possible.

3.2   Layout of optical components: distances and focal lengths

To minimize the aberrations resulting from focusing optics a 2:1 ratio between the source – mirror and mirror - sample distance for the HP/SC station was chosen.

From this it follows for the positions of the optical elements:

ID center:	0m
Gate valve of front end (FE):	18.2m
M1 collimating mirror:	20m
CCM Channel-cut monochromator:	22m
M2 horizontally focusing mirror:	24m
KBV:	33.5m
KBH:	33.9m

HP / SC station 1:	36m
PD station 2:	39m
Mirror glancing angle:	2mrad
	3mrad maximal
	(3.5mrad for the focusing mirror M2)

The second mirror, M2, is a cylinder mirror used for partial horizontal focusing on station 2, PD, and focusing on station 1, SC/HP. It has sagittal curvature. To realize this with only one mirror a compromise for the radius of curvature has to be found. A sagittal curvature of $R_{sagittal}$= 48mm or 50mm is suggested. This keeps beam size, shape and divergence at the PD station at acceptable values and allows for focusing at station 1 under an increased glancing angle of 3-3.3mrad transmitting a maximum energy of about 26-27keV.

$$R_{meridional} = \frac{2}{\sin\theta}(\frac{pq}{p+q}) \qquad R_{sagittal} = 2\sin\theta(\frac{pq}{p+q}) \qquad \text{[Eq.3.1, e.g. Patterson05]}$$

p: source - mirror distance

q: mirror - sample distance

θ: mirror grazing angle

For the collimating mirror q → ∞ and the sagittal curvature is:

$$R_{mer,coll} = \frac{2p}{\sin\theta} \qquad \text{[Eq. 3.2]}$$

(In case of a vertically collimating/refocusing mirror pair the distance between both mirrors doesn't add to the optical path.)

Station 2 (PD) is located 39m from the source. With $R_{sagittal}$ =48mm and θ=2mrad the focal distance (1:1 focusing) is 48m, thus preserving the horizontal divergence at the sample position. Taking into account the divergence of the beam and the position of the station at 39m the horizontal beam width is reduced by a factor of about 4.3 compared to the unfocused beam. A sagittal curvature of 48-50mm keeps horizontal beam size and divergence at reasonable values (see section 4.2.8). The influence on the vertical divergence is only minimal then and can further be reduced by closing the slits in front of M2 horizontally.

Station 1 (HP / SC) is located 36m from the source leading to a demagnification of M=p:q=2:1. At this position the errors introduced by a focusing toroidal mirror (like astigmatism and coma) are minimal. To get a spot size of about 0.3 x 0.3mm^2, the before mentioned cylindrical mirror M2 ($R_{sagittal}$=48mm) has to be tilted from 2 to 3mrad and meridionally bent to a curvature of about 9km, as can be found by ray-tacing. Due to the increased mirror angle the accessible energy range is then reduced to about 27keV.

3.3 Working configurations of the optical elements

The reflectivity of the mirror coating restricts the accessible energy range. The coating materials are chosen to cover the range between 8 – 40keV with a constant angle of 2mrad for both mirrors.

Therefore, we plan for two main configurations of the optical elements:

Mirrored mode:	8 - 40keV.
Un-mirrored mode:	> 40keV

In both modes the KB-multilayer mirror can be used as additional focusing option. The KB-mirror will be placed 2 to 2.5m upstream station 1 focusing the beam between 20 and 50keV, thus covering the high energy region for HP experiments.
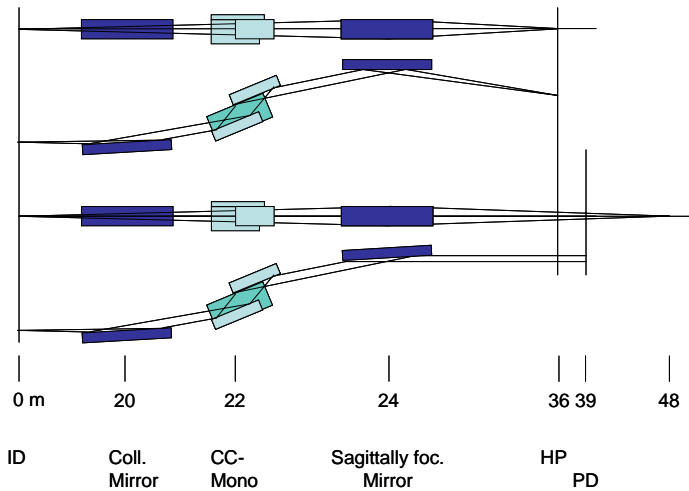
Figure 3.1 (I) Mirrored mode with focus on station 1, E_{phot}: 8 - 27keV (top and side view)
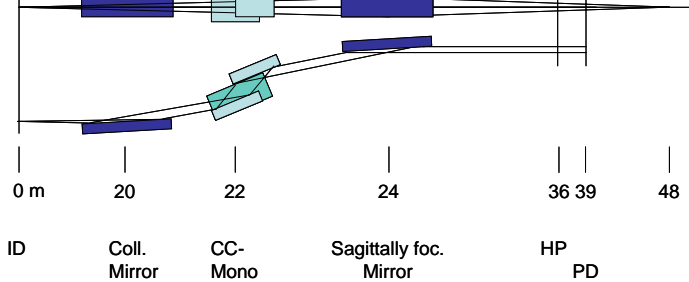
Figure 3.2 (II) Mirrored mode with partial horizontal focusing (station 1, 2) E_{phot}: 8 - 40keV
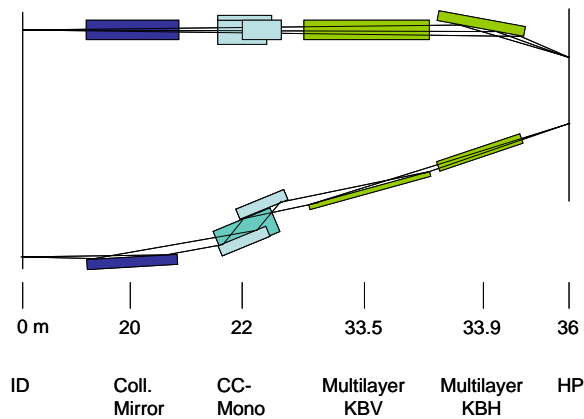
Figure 3.3 (III) Mirrored mode with multilayer KB-optics, E_{phot}: 20 - 40keV
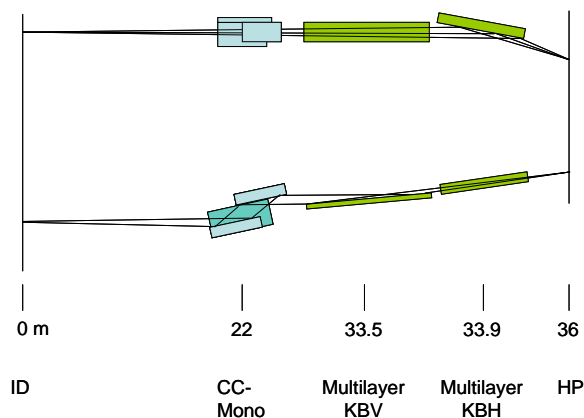
Figure 3.4 (IV) Un-mirrored mode with multilayer KB-optics, E_{phot}: > 40keV.
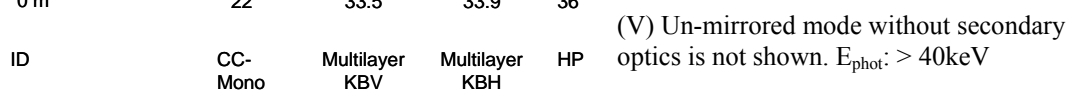
(V) Un-mirrored mode without secondary optics is not shown. E_{phot}: > 40keV

3.3.1 Mirrored mode

The energy range in the mirrored mode is defined by the mirror coating and grazing angle. To cover a wide energy range without the need of major realignments the mirrors will be operated at a fixed glancing angle of 2mrad. In the mirrored mode a bendable collimating mirror upstream the monochromator and a bendable cylinder mirror

downstream the monochromator are inserted into the beam path. Three different coatings (Si, Rh, Pt or Ir) on the collimating pre-mirror adapt for the different energy ranges. The second mirror is Pt (or Ir) coated. The maximum allowed angle for both mirrors is 3mrad and 3.5mrad, respectively. The small angle of the collimating mirror allows for a liquid metal contacted external cooling with the cooling pipes in a GaIn (Galinstan) filled bathtub. Equal angles for first and second mirror allow for a horizontal beam at the PD station. All mirrors can be inserted and removed independently, thus giving a huge flexibility of tailoring the beam at the sample position.

The mirrored mode, in particular mode II, will serve about 80% of the applications. Mode II is also standard setup for powder diffraction. Keeping both mirrors at the same angle reduces the effort for alignment at different energies.

3.3.2 Un-mirrored mode

The un-mirrored mode is used for high energy applications around 50keV. For energies above the transmitted range of the mirrors the monochromator can directly be operated in the beam. As this is a high energy (high K-value) setting the white beam slits have to be set to a reasonably small value. In this configuration the KB-system will be used as focusing device.

4　Expected beam line performance

4.1　Heat loads and flux in operating conditions

A very important issue at this beam line is the accepted total power and power density in the optical components. In particular three parameters define heat load and flux transferred to the optics: apertures, transmittance of filters and K-value of the source. The usable range of these parameters is determined by the maximum heat load that the optical elements can handle. Typical values and the usable ranges of these parameters are presented bellow.

Vertical aperture:

The vertical aperture is defined by the acceptance of the collimating mirror which is typically 125µrad (1.2m mirror length @ 2mrad grazing angle) resulting in 2.4mm beam height. The maximum aperture of 180µrad applies for low K-values and 3mrad grazing angle (low energy regime) and is not a typical setting.

The vertical aperture in the un-mirrored high energy setting is defined by either the acceptance of the monochromator and multilayer optics, the vertical beam size at the sample position or the acceptable heat load on the first monochromator crystal. The latter can of course be adapted by the white beam filters. The aperture in the un-mirrored setup always stays below the value of the mirrored beam.

Horizontal aperture:

In most cases a horizontal aperture of 1000µrad implies that the first pre-filter has to absorb more than 550W, which is a very high value (this already happens for the nominal storage ring current of 250mA.) thus the maximum horizontal aperture is 1000µrad. The typical value is 600µrad.

Filters and vacuum windows

Two different ways to separate the beam line from the front-end (FE) and storage ring vacuum are possible: The conventional way by using a Be-window and if necessary Be or graphite pre-filters and alternatively CVD-diamond windows of about 0.3mm thickness, that are increasingly employed at sources like ESRF for undulator beams. A third, mirrorless variant employing differential pumping is not relevant, since the thereby accessible low energy region is not needed at this beam line.

A solution with Be-window and pre-filter is preferred, followed by a variable white beam filter box (see section 4.2.3).

Absorbed power on mirror

Due to the small glancing angle the fraction of the total power passing through the aperture and being absorbed in the pre-mirror is rather low. Besides, the power absorbed in the pre-mirror depends on the selected coating material and thus on the energy range. In all cases considered the maximum absorbed power can be kept below 1kW.

Absorbed power on monochromator

The maximum accepted power on the 1st monochromator crystal is still under investigation. As design criterion a maximum power of about 650W on the first monochromator crystal is chosen (see section 4.3). Both monochromator crystals will be externally cryo-cooled to reduce the influence of thermally induced distortion. Literature addressing this problem report different values for acceptable heat loads and propose different cooling schemes (e.g. Tajiri01, Zhang03, Chumakov04). One of the most optimistic estimations is given by Chumakov: "indirectly cooled silicon monochromators can provide an ideal performance up to a heat load of 400W and an acceptable performance at 900W". In his analysis no influence on the Si 111 reflection at 14.4keV was found up to a heat load of 900W.

Source Power Density

Table 4.1: Power density in normal incidence [W/mm^2] of the ID with no filtering. Only some values are exemplarily given.

Distance to ID (m)		18	19.5	20.5	21.5
K: 6.08	400mA	138	118	106	97
K: 6.08	250mA		73.8		
K: 3.65	400mA		70.6		
K: 3.65	250mA		44.2		

Heat loads on the optical components

Power absorbed by the optical components has been calculated for a number of representative working conditions and are summarized in the following tables (table 4.2 – 4.5). Some extreme but realistic configurations are marked in yellow. Configurations used to calculate heat load effects are marked in green. Critical values, that means technically too difficult or with non-acceptable performance, are marked in red.

Table 4.2, 4.3, 4.4 and 4.5 abbreviations:

Apert: Power passing through aperture
C: Pyrographite filter (with thickness in mm)
D: Diamond filter
Be: Beryllium window
Si, Rh, Pt: Mirror with respective coating
Mono: 1st monochromator crystal

K	H_{Div} [µrad]	ID total	Apert	C0.3	C1.0	Be0.3	C1.0	C3.0	C4.0	Si	Mono	Rh	Mono	Pt	Mono
3.65	600	4280	1111	355	228	11	-	-	-	280	237	64	454	54	463
	1000	4280	1693	592	354	16	-	-	-	374	358	81	651	73	659
6.08	600	11877	1897	328	292	19	-	--	--	939	319	390	868	272	986
	600	11877	1897	328	292	19	159	288	-	709	102	316	495	211	600
	1000	11877	3079	550	483	32	260	468	359	859	71	401	529	261	669

Table 4.2: Phase 1: Synchrotron beam current I = 250mA, V_{Div} = 122µrad, absorbed power in the respective element given in Watt.

K	H	ID	Apert	C0.3	C1.0	Be0.3	C1.0	C1.5	C3.0	C4.0	Si	Mono	Rh	Mono	Pt	Mono
3.65	300	6850	917	284	447	9									47	391
	400	6850	1213	378	246	12					317	259	74	502	62	514
	600	6850	177	568	364	17					448	380	102	726	84	741
6.08	300	19000	1524	260	233	15					762	254	320	695	225	791
	300	19000	1524	260	233	15		176							203	636
	400	19000	2040	349	313						1027	350	429	949	300	1078
	400	19000	2040	349	313	21	170		310		769	109	345	532	231	646
	600	19000	3026	525	468	31	254		461	357	872	69	416	525	273	669

Table 4.3: Phase 2: Synchrotron beam current I = 400mA, V_{Div} =122µrad, absorbed power in the respective element given in Watt.

K	H	ID	Apert	D0.3	D0.3	Be0.3	C1.0	C3.0	C4.0	Si	Mono	Rh	Mono	Pt	Mono
6.08	300	19000	1524	316	111	-	-	-	-	791	305	331	765	223	863
	400	19000	2040	425	150	-	346	-	-	914	205	393	726	269	850

Table 4.4: Phase 2: Synchrotron beam current I = 400mA, V_{Div} =122µrad, absorbed power in the respective element given in Watt using diamond filters:

K	H_{Div}	V_{Div}	ID	Apert	C0.3	C1.0	Be0.3	Mono
6.08	60	120	19000	294	50	45	3	197

Table 4.5: Phase 2: Synchrotron beam current I = 400mA, V_{Div} =120µrad, absorbed power in the respective element for the 50keV case with KB-mirror:

Absorbed power densities in filter elements [W/mm^2] in worst case, K=6.08, I=400mA:

Pre-filter 1 (0.3mm Pyrographite)   18.6

Pre-filter 2 (1.0mm Pyrographite)   17.1

Be vacuum window   1.2

First white beam filter (1mm Pyrographite): 9.5

Flux

In figure 4.1 the photon fluxes Ph/sec/0.1%BW through a fixed aperture for two K-values are given. Top: 600x125µrad^2, 250mA. Bottom: 600x125µrad^2, and 400x125µrad^2, 400mA. The fluxes are attenuated by Pyrographite filters as described before. The figures show that a reduced K-value increases the performance at low energies.
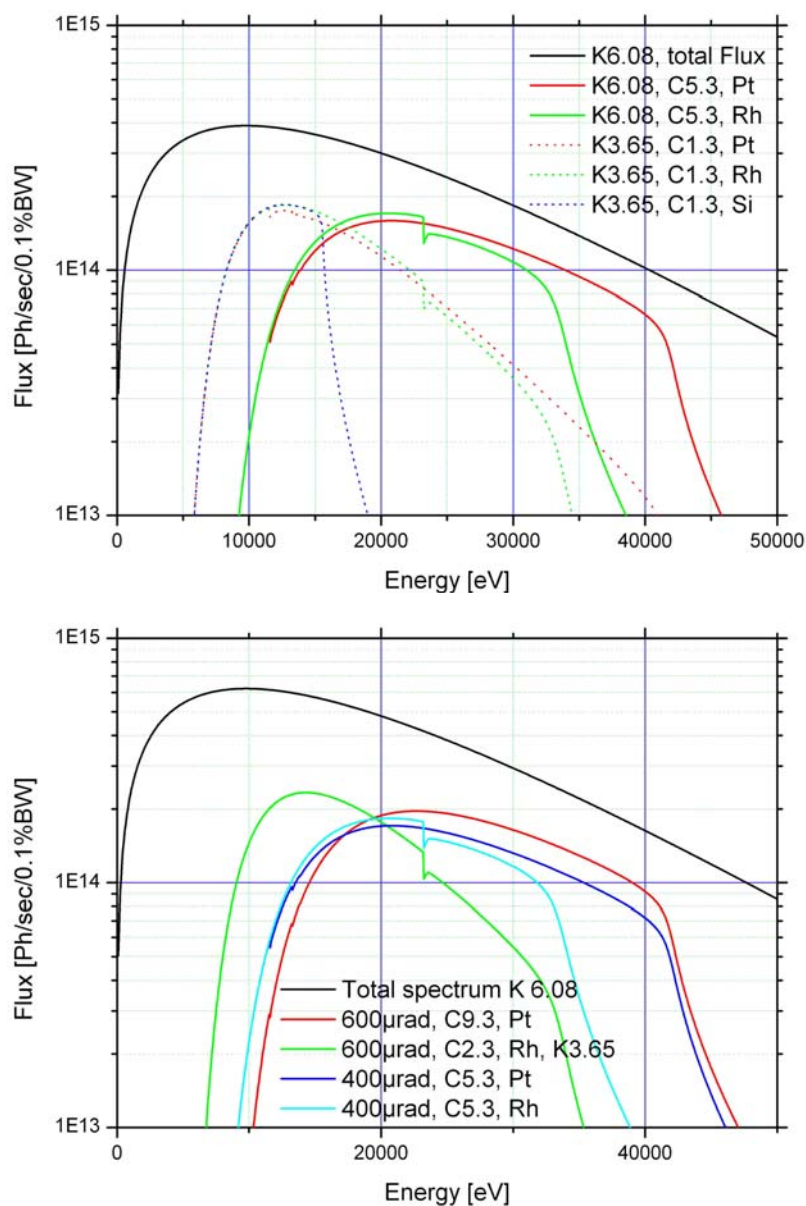
Figure 4.1: Photon flux Ph/sec/0.1%BW at different operational conditions (horizontal divergence, K-value, C-absorber thickness in mm and mirror coating).

4.2 Ideal optics performance

4.2.1 Energy ranges and harmonic suppression:

Figure 4.2 shows the transmitted flux for different M1 mirror coatings at 2mrad glancing angle at K=6.08 (Si-mirror @ 3mrad and K=3.65). From this figure the useful energy ranges can be inferred. Ideal conditions were assumed.
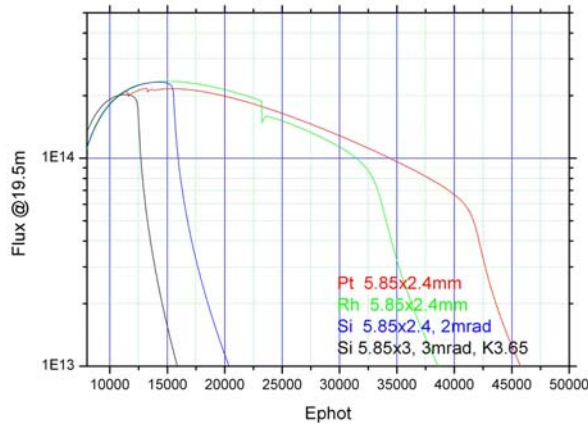
Useful energy ranges and coatings for the collimating mirror:

8-15keV   Si

14-22.5keV Rh

22-40keV   Pt

Figure 4.2: Flux behind M1 positioned at 19.5m with slit sizes corresponding to an aperture of 300x123µrad^2 (see text).

Harmonic suppression

The ratio of the harmonic suppression through the optical components depends solely on the mirrors coating material and on the monochromator crystals. The higher harmonics contamination ratio was calculated with XOP by normalizing the number of photons transmitted at the distinct energies and assuming the following working condition: K: 6.08, H: 300µrad, θ_i: 2mrad, Filter: 0.6mm diamond, 1st mirror according to energy range, 2nd mirror always Pt coated (see figure 4.3). The effect of the crystals is not considered in figure 4.3.
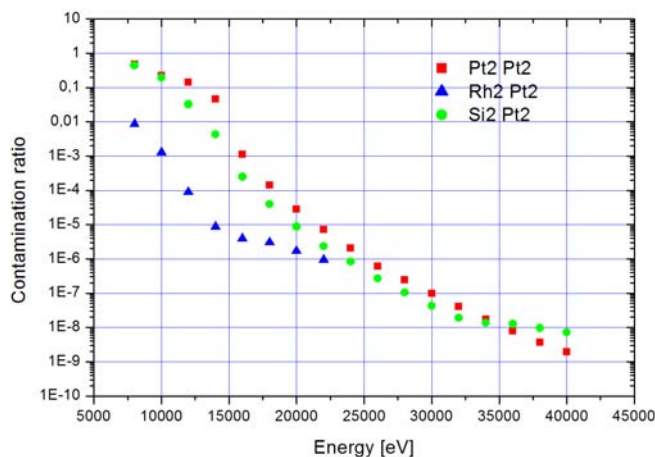
Figure 4.3: Higher harmonics contamination ratio of two mirrors at 2mrad glancing angle and respective coating (see text).

Table 4.6: Integrated reflectivities for different reflections and corresponding harmonics at 8keV [Caciuffo87].

Integrated intensity $I_h^{(n)}$ for harmonic reflection in perfect Si crystal in symmetric Bragg geometry for σ polarized incident beam; $\lambda_1 = 1.6$ Å. Although the highest intensity is delivered by the (111) reflection, the (331) or the (511) reflections are preferable when a harmonic free monochromatic beam must be obtained (from ref. [114])

h	k	l	n	$I_h^{(n)}/I_h^{(1)}$	$I_h^{(n)}/I_{111}^{(1)}$
1	1	1	1	1.0	1.0
3	3	3	3	0.0672	0.0672
4	4	4	4	0.0384	0.0384
5	5	5	5	0.0119	0.0119
2	2	0	1	1.0	0.7769
4	4	0	2	0.1633	0.1268
6	6	0	3	0.0405	0.0314
8	8	0	4	0.0121	0.0094
3	1	1	1	1.0	0.4379
9	3	3	3	0.0314	0.0138
12	4	4	4	0.0126	0.0055
4	0	0	1	1.0	0.4190
8	0	0	2	0.1193	0.0611
12	0	0	3	0.0219	0.0112
3	3	1	1	1.0	0.3196
9	3	3	3	0.0184	0.0058
12	12	4	4	0.0065	0.0021
4	2	2	1	1.0	0.4190
8	4	4	2	0.0904	0.0379
12	6	6	3	0.0143	0.0060
5	1	1	1	1.0	0.2806
15	3	3	3	0.0122	0.0034
20	4	4	4	0.0039	0.0011

Figure 4.3 shows that higher harmonics are sufficiently suppressed by any mirror combination at energies above 20keV. Between 10-20keV Si or Rh stripes on the collimating mirror have to be used. In the high-energy non-mirrored mode the decrease in the ID spectrum, suppression by mono-crystal detuning (max: $2 \cdot 10^{-2}$) and suppression by the KB multilayer is effective. Table 4.6 gives the integrated intensities for certain reflections and their harmonics transmitted by the monochromator at about 8keV.

4.2.2 Energy resolution and vertical beam divergence

The energy resolution of the beam line is given by

$$\frac{dE}{E} = ctg\,\theta_M \cdot \sqrt{\Delta\theta_D^2 + V_{Div}^2} \; , \qquad\qquad \text{Eq. 4.1}$$

where θ_M is the monochromator angle, $\Delta\theta_D$ is the Darwin width of the crystal and V_{Div} the vertical beam divergence.

The beam line will deliver high resolution powder diffraction data, which means that the energy resolution must be of the order of $dE/E = 2 \cdot 10^{-4}$. Additional broadening has to be added quadratically in the square-root expression, assuming a Gaussian distribution. While the Darwin width of the monochromator crystal is typically very narrow (Figure 4.4), the vertical divergence of the ID is not and thus makes vertical collimation necessary. Collimation in this beam line will be realized by a mirror with adaptable mirror bender bending the whole pre-mirror to a curvature of 20km in the ideal case. Optimum collimation is achieved by a parabolic mirror, which is often approximated by a cylindrical shape leading to small aberrations only, due to the large radius of curvature. Since bender mechanisms for parabolic/elliptic bending are usually more stable against heat load and drifts than bender with a single actuator (giving cylindrical shape), this type will be used in the setup. This implies that it might be possible to give the mirror a parabolic shape. However, calculations were done assuming cylindrical shape.
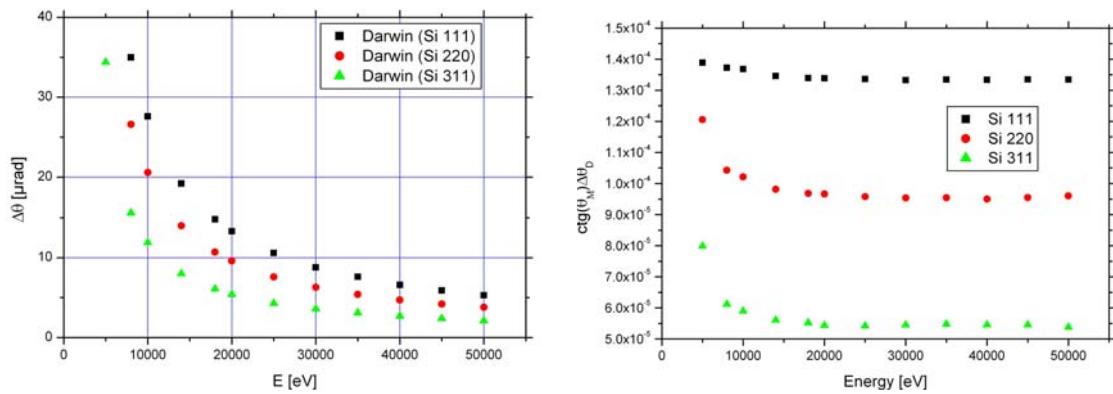
Figure 4.4: Left: Darwin width for different Mono-crystal reflections at different energies. Right: Darwin width multiplied by the ctg of monochromator angle vs. energy.

Table 4.7 summarizes the effect of the vertical divergence (emerging from the finite source size) on the energy resolution. Values were taken from ray-tracing calculations assuming ideal optics. The resolution stays within reasonable values.

Energy	V_{div} [μrad]	dE [eV]	dE/E
10keV	7.4	1.3	$1.3 \cdot 10^{-4}$
20keV	5.2	2.7	$1.35 \cdot 10^{-4}$
30keV	4.3	4.1	$1.4 \cdot 10^{-4}$
40keV	4.0	5.4	$1.4 \cdot 10^{-4}$

Table 4.7: Residual vertical divergence resulting from finite source size and maximum resolution: K-value = 6.08, mirror angle=2mrad, radius of curvature=20km.

The heat introduced by the beam creates a deformation of the ideal shape (slope error) which (in the mirror) can partly be compensated by changing the bending radius of the mirror. The residual slope error due to non-uniform heat distribution ("thermal bump") increases the vertical divergence upstream the monochromator ($+(2.354*\sigma_{RMS})^2$) and hence deteriorates the energy resolution. Slope errors from manufacturing and bending are typically below 2μrad rms for mirrors of 1100mm optical length and are of minor importance compared to the "heat bump" (see section 4.3).

In the case of the monochromator the heat problem is met by cryo-cooling: At liquid nitrogen temperatures the thermal conductivity of silicon is considerably increased and its thermal expansion is zero at 125K. The interesting ratio between thermal expansion and conductivity α/k is zero at 125K and about 50 times smaller at 77K than at RT [Zhang03]. Accordingly, heat can faster be removed from the crystal and a temperature gradient has smaller influence compared to RT. Unfortunately, this gain is compromised by lower heat capacity of lN2 compared to water (higher flow rate and vibration) and the bad heat transfer coefficient between silicon, crystal holder and coolant. However, the heat load on the optical elements should be kept as low as possible.

The second horizontally focusing mirror will be equipped with a bender allowing focusing on the SC/HP and the PD station. According to Gozzo06 vertical focusing on the sample position influences the instrumental resolution function of the PD station described by:

$$\Delta^2(2\theta) = (\Delta\tau_p^2 + \Delta_m^2/2)(\tan\theta_a/\tan\theta_m - 2\tan\theta/\tan\theta_m)^2 + \Delta_a^2 + \Delta\tau_f^2 \qquad \text{Eq. 4.2}$$

with:

$\Delta\tau_p$ vertical divergence of collimated beam

Δ_m Darwin width of monochromator

θ_m Bragg angle of monochromator

θ_a Bragg-angle of analyzer crystal (detector)

Δ_a Darwin width of analyzer crystal

$\Delta\tau_f$ vertical divergence of the focusing mirror

Even without bending the second mirror partly transfers the horizontal divergence into the vertical (diffraction) plane leading to asymmetric reflections. This effect can be reduced by closing the horizontal slits in front of M2 (or M1) or even by removing the mirror.

The influence on the instrumental resolution function for a flat and bent second mirror is given in section 4.4

4.2.3 Filter

Besides toxicity, Beryllium vacuum windows can have fluctuations in thickness and density leading to a loss of coherence of the beam and an additional blur of the spot. Although this can be reduced by polishing, CVD-diamond windows typically show better performance [Espeso98]. On the other hand, diamond vacuum windows are several times more expensive and not well established for large apertures. Considering the rather large source size and divergence of the ID, the separation of the beam line from the front-end region should be realized by a Be-window. This window then has to be protected by two consecutive water-cooled pyrographite filters of 0.3mm and 1.0mm thickness upstream the window. Since water cooling requires proper clamping, the buckling due to the temperature gradient might break the filter. An alternative solution exists in radiation cooled pyrographite (or Sigradur©) spring-clamped to a water cooled metal frame.

For calculations in this section the thickness of the pre-filters is chosen to absorb a little more than 500W at most conditions. This is a value that can be handled by commercially available devices. Proper thicknesses have to be chosen in cooperation with the manufacturing company. Besides, FEA calculations are planned to investigate the behavior of the filters.

The pre-filter/vacuum-window combination is followed by a white beam filter consisting of three vertically movable rods holding three water cooled absorber foils and one empty window each. The empty window allows for the non-attenuated beam, the other absorber foils still have to be specified. A possible filter window combination is given below. The filter box is preceded by two fixed pre-filters (0.3mm and 1.0mm Pyrographite) and the Be-vacuum window.

C0.3mm C1.0mm Be0.3mm	C1mm	C3mm	C4mm
	C0.5mm	C1mm	C3mm
	C0.3mm	C0.5mm	C1mm
	empty	empty	empty

4.2.4 Collimating pre-mirror M1

M1 is an upwards reflecting, high heat load mirror to collimate the beam in the vertical plane. It's therefore water cooled and made out of material with good thermal properties (low thermal expansion and high conductivity). The absorbed power, of course, strongly depends on the actual beam line setting, but can always be adapted by the white beam filters preceding the mirror. Since the energy range of the beam line is above 8keV, stripping off the low energy fraction of the ID spectrum with low-Z absorbers has only little influence on the actually used part of the spectrum. The grazing angle of the mirror is 2mrad, allowing for a transmitted energy up to 40keV (Pt-coating). The smallest angle for a mirror found in literature is ~1.6mrad [Masson03] and was applied at the former ESRF powder diffractometer BM16 to a Rh-coated collimating pre-mirror.

One issue that should be considered by the manufacturer during the construction of the mirror is the heat load resulting from Compton scattered radiation. The ID spectrum considerably contributes at very high energies, whose scattered radiation potentially heats vessel and mirror mechanics directly.

According to the calculations in section 4.1 the maximum absorbed power in realistic cases can be kept below 1kW. Furthermore, this high heat load only exists in the low-energy setup, where the energy resolution is less affected due the rather broad Darwin widths of the monochromator crystals. Due to source size (section 2) and distance ID-M1 (section 3) the minimum achievable vertical divergence is about 4-7μrad.

The length of the mirror makes compensation of 'gravity sag' necessary. This can not be completely corrected by the bender.

Calculations on the effect of heat load (section 4.3) show that externally cooling is sufficient, if the cooling pipes are contacted by a liquid metal (Galinstan) in a bathtub close to the exposed surface. Since the mirror angle is kept below 3mrad this seems technically feasible. Possible mirror materials are Glidcop (Cu/Al_2O_3) and single crystal silicon, whereas the latter is preferred due to lower costs and better surface finish. The upstream side of the mirror is protected from the photon beam by a water cooled Cu-plate. Figure 4.5 shows a proposed mirror cross section.

Figure 4.5: Proposed cross-section of the mirror showing also the cooling pipes.

M1 Distance to source: 20m

Total length: 1200mm

Optical length: 1100mm

Number of reflecting stripes: 3 (Si, Rh Pt)

Width of each stripe: 20mm

Distance between stripes: 5mm

Cooling scheme: Externally cooled (see text)
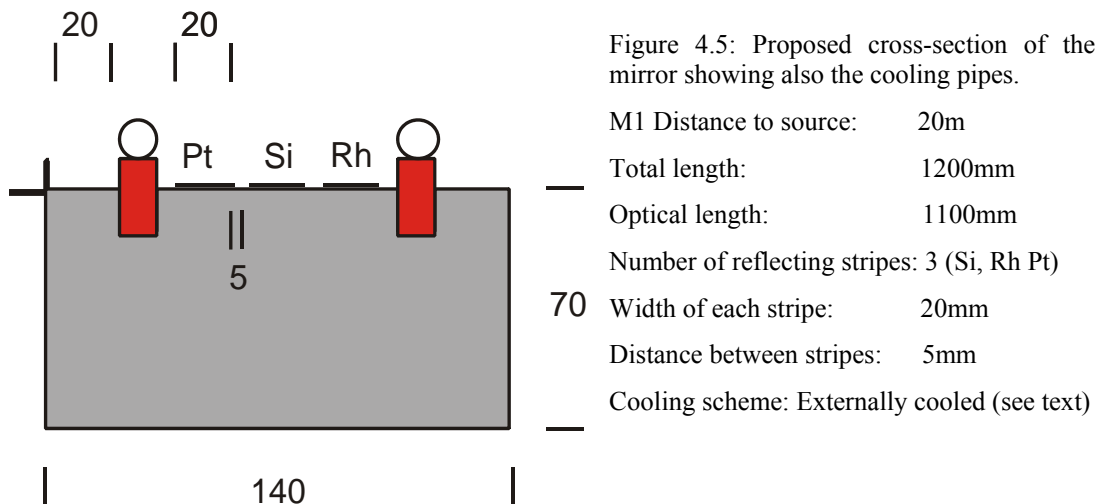
4.2.5 Channel-cut monochromator CCM

The monochromator consists of two flat crystals in Bragg reflection-geometry and non-dispersive (+,-) setting. It can principally be designed either as Double-Crystal monochromator DCM or as Channel-Cut monochromator CCM. In the DCM both crystals sit on separate stages and can individually be aligned. The geometric shape is rather simple and the crystals can be quite big. Measures have to be taken to keep the second crystal at the same temperature as the first. A CCM is cut out of a single crystal block. Maximum size (and cost) is related to the diameter of the silicon ingot the monochromator is cut out of.

Beside better cost effectiveness other reasons to use a CCM design are:

- Reduced mechanical complexity avoids drifts and vibrations

-The directly connected crystals give better (and faster) thermal equilibration and therefore smaller deviation in d-spacing between both crystals.

The necessary detuning of the second crystal is in the CCM accomplished by the connection of both crystals with a "weak link" and a "pusher" for the second crystal avoiding bending of the latter when it's detuned. The appearance of "glitches" or "Laue-spots" during scanning is not an issue as the monochromator is mainly used at fixed energies and only scanned over ranges of about 100eV. Besides, parasitic reflections close to the primary beam can be avoided by setting slits downstream the CCM or slightly changing the energy.

Considering all of this a CCM design is preferred. Both crystals should be externally cooled by liquid nitrogen (cryo-cooling).

The reflecting surfaces of the CCM routinely used are cut in Si [111] direction. To get higher Bragg-angles for the crystals at high energies and to increase energy resolution a second monochromator crystal with Si 311 surface should be placed next to it. Both crystals are interchanged either by translating the crystal stage inside the vessel or the whole vessel with respect to the beam.

Figure 4.6 shows a drawing of a CCM together with its cooling pads. This design is used at several ESRF beam lines.
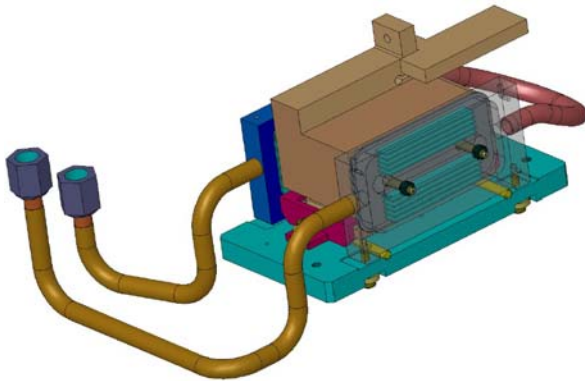
Figure 4.6: CCM with cooling pads. This design is used at several ESRF beam lines

Dimensions:

The dimension of the monochromator crystals is defined by the total heat that has to be removed requesting sufficient contact surface, a lateral "moderation" between hot spot and cold cooling contact also defining the deformation of the crystal and by the beam dimension and Bragg angle. When changing the energy the fixed gap in the CCM design leads to a change of the height of the exiting beam, which is getting less pronounced with smaller gap and higher energies. The CCM can be designed with its rotational axis either lying on the surface of the first crystal, or between both crystals. In the first case the beam moves along the second crystal, when the energy is changed, in the second case this movement is partly transferred to the first crystal, depending on the exact position of the pivot axis between both crystal surfaces. The latter option is preferred with the axis lying half way between the surfaces. In this case the length of the second crystal can considerably be shortened, reducing effects of vibration and increasing the size of the first crystal that has to be large enough for cooling reasons, anyway.

The beam travel along the crystals increases considerably with wider gap. On the other hand, a smaller gap introduces difficulties during alignment and operation and necessitates complex measures to separate Bremsstrahlung (BS) from the exiting beam. The latter will be accomplished by a tungsten block with (approx.) 100mm in diameter and 200mm in length with a 5x25mm^2 opening parallel to the axis, but offset by about 7mm (a proper design still has to be defined). This block will be placed immediately behind the monochromator and although probably not fulfilling requirements for personal

safety it will reduce the amount of background in the experimental hutch. To ease the initial alignment of the monochromator it should be movable in height allowing to see the direct beam.
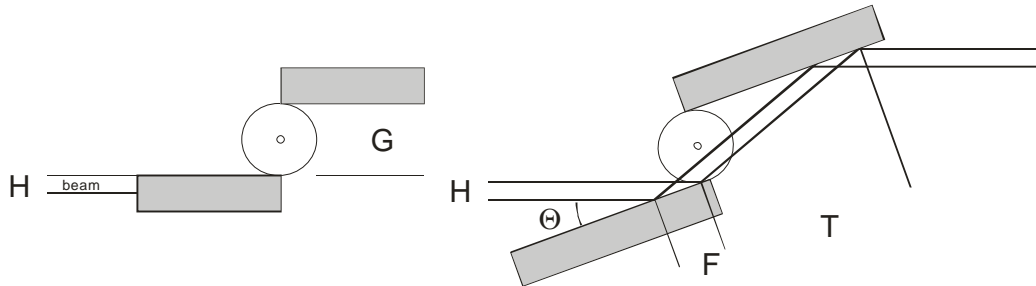
Figure 4.7: Beam travel on the monochromator crystals.

The expressions to calculate footprint and beam travel are

$$F = \frac{H}{\sin\theta} \quad , \qquad\qquad T \approx \frac{G}{\tan\theta} \qquad\qquad\qquad \text{Eq.: 4.3}$$

where G=gap distance, H=beam height, F=beam footprint and T=distance traveled from first bounce impact to second bounce impact

Beam dimensions on the monochromator crystals in the Si 111 case:

Gap   4mm

Change in beam height (8 - 50keV)   :   0.2mm

Maximal horizontal beam width (@22m, 1000µrad)   22mm

Table 4.8: Minimum dimensions of the Si111 monochromator crystals for a 4mm gap and 2.5mm beam height when working in the 8-50keV energy range.

E (keV)	Bragg angle (°/rad)	1st crystal length (footprint of the beam)	Min length of 2nd crystal (footprint plus beam travel)	Min total length of crystal block
50	2.3/0.04	62.5mm	100mm	162.5mm
40	2.84/0.05	50mm	80mm	130mm

4.2.6 Horizontally focusing cylinder mirror M2

The second mirror is a horizontally focusing mirror with cylindrical shape and the cylinder axis parallel to the beam direction (sagittal curvature). As mentioned in section 3 the radius of curvature is 48mm (or 50mm) imaging the source 1:1 at 48m when set to a grazing angle of 2mrad. It is Pt coated and (for the PD station) stays at the same angle for all energies. Small alignment corrections are necessary when changing the energy due to the non-zero shift in beam height. The mirror is equipped with a bender (∞ to ~5km) so that vertical focusing on station 1 and 2 is possible.

Although removable this mirror is standard setup for the PD station at 39m. The distances of the particular elements lead to a horizontal demagnification compared to the un-mirrored beam at the sample position of 2.7 ($R_{sagittal}$=48mm). The horizontal beam sizes and divergences in both directions (resulting from ray-tracing) are given in section 4.2.8.

4.2.7 KB-mirror system

The KB-mirror system is the main focusing optics for the HP station. It's used in the energy range between 20-50keV and must therefore be coated with a suitable multilayer with low d-spacing. For HP experiments at pressures above 20GPa, as well as experiments using laser heating, the DACs have very small apertures and sample area of the order of 40˚ and 20μm, which is the required spot size. On the other hand, very low divergence is necessary for powder diffraction under these conditions, about 1mrad maximum, that should ideally be the same in horizontal and vertical direction to make the integration of 2-dimensional detectors easier. The rather big source size (section 2) compromises either spot size or divergence. In addition to this increases a long secondary focal length the sensitivity of the system to vibrations. The proper type and length of the multilayers still has to be decided.

Shadow ray tracing calculations are presented with the following parameters:

Optical layout:

ID K=6.08	0m	
Mono Si 111	22m	
KBV	33.5m	300mm length
KBH	33.9m	300mm length
HP	36m	

Multilayer used for calculation:[Mo/B$_4$C]$_{50}$ on Si substrate, $D_{doublelayer}$=20Å, γ=0.5 (not appropriate for 3rd harmonic suppression), no lateral D-grading

Demagnification:

M_V=p_v/q_v	13.4
M_H=p_h/q_h	16.1
Spot size (V x H):	7x36μm
Divergence (V' x H')	930x1110μrad

1-dimensional micro-slits in front of each mirror shall be provided to reduce the aperture. A "clean-up" pinhole should be available directly in front of the sample.

4.2.8 Beam characteristics at the experimental station

Efficiency of the optics

The total number of photons was estimated using the ray-tracing program SHADOW and XOP/WS [Sanchez del Rio97] to calculate the efficiency of the ideal optics. The following values are used:

Horizontal aperture:	1000µrad, 600µrad, 400µrad.
Vertical aperture:	defined by the collimating mirror M1 at 2mrad glancing angle and 1100mm optical length (110µrad)
Reflectivity:	three coatings (Si, Rh, Pt) with 100% density calculated with the SHADOW preprocessor prerefl.exe.
Divergence of the ID:	Calculated with SPECTRA for K 6.08 and 3.65 (section 2).
No slope error or roughness is assumed.	

The number of photons per second at the sample position N is: $N = T \times \text{Flux} \times 1/dE_{BW} \times dE_{crystal}$

T: transmitting efficiency= $I_{shadow}/I_0 * dE_{source}/dE_{crystal}$ from the SHADOW program

Flux: Integral Photon Flux of the ID at the respective energy in Ph/sec/0.1%BW

dE_{source}: Bandwidth of the source used for calculations

$dE_{crystal}$: Bandwidth transmitted by the monochromator

Table 4.9: Efficiency, size and divergence at the sample position for different configurations from ray-tracing. Values for M2: $R_M = \infty$, $R_S = 5$cm.

Powder Diffraction Station

K	H (µrad)	E (keV)	T	Hdiv (µrad)	Vdiv (µrad)	Hsize (mm)	Vsize (mm)	Beam width, no foc. (mm)
3.65	1000	10	0.29	520	7.0	6.0	2.0	26
		20	0.55	468	5.3	5.4	2.0	23
		30	0.56	450	4.5	5.1	1.9	21
		40	0.49	431	3.9	4.8	1.9	20
	600	10	0.22	513	6.6	5.3	2.0	22
		20	0.44	462	4.9	5.1	1.9	22
		30	0.46	447	4.3	4.9	1.9	20
		40	0.42	434	3.8	4.8	1.8	19

	400	10	0.17	362	6.2	3.8	2.1	**15**
		20	0.33	361	4.6	3.7	2.0	**15**
		30	0.35	360	3.9	3.7	1.9	**15**
		40	0.32	360	3.5	3.7	1.9	**15**
6.08	**600**	10	0.10	543	8.7	5.5	2.0	
		20	0.23	543	6.6	5.5	1.9	
		30	0.25	541	5.6	5.5	1.9	
		40	0.23	539	5.0	5.5	1.9	**23**
	400	10	0.07	366	8.1	3.9	2.1	15
		20	0.16	366	6.0	3.7	2.1	15
		30	0.17	367	5.0	3.9	2.0	15
		40	0.16	366	4.5	3.8	2.0	15

Single Crystal station

3.65	**600**	20	.48	1046	140	.3	.3	
		20	.002	12.4	4.6	.5	.5	No mir. M2

Flux at sample:

Table 4.10: Total monochromatic flux at the sample position for different configurations.

Powder Diffraction Station

K	I(mA)	H(μrad)	Filters	E(keV)	Flux$_{Mono}$ Ph/sec
3.65	**250**	600	C1.3Be0.3	10	**1.1e13**
				20	**5.6e12**
				30	**1.1e12**
				40	**2.3e11**
	400	400	C1.3Be0.3	10	**1.4e13**
				20	**6.7e12**
				30	**1.4e12**
				40	**2.5e11**
		600	C2.3Be0.3	10	**1.1e13**
				20	**8.1e12**
				30	**1.5e12**

				40	3.5e11
6.08	250	600	*C*5.3Be0.3	10	1.7e12
				20	9.2e12
				30	3.9e12
				40	1.3e12
	400	400	*C*5.3Be0.3	10	1.9e12
				20	1.0e13
				30	4.3e12
				40	1.4e12
		600	*C*9.3Be0.3	10	3.2e11
				20	9.9e12
				30	4.9e12
				40	1.7e12

Single Crystal Station

3.65	250	600	with 2nd mirror (0.3x0.3 mm^2 spot size) R_S=5 cm, R_M=9km	20	6.1e12
			Without second mirror (0.5x0.5mm^2 spot size)	20	2.6e10

KB-mirror @HP station

3.65	250	600	Without M1, 7x36μm	40	1.5e10

Spot size and shape

Table 4.11: Beam spot at PD station with different H_{div} using M2 as cylinder mirror with infinite meridional curvature and R_S=5cm.

K=6.08, E=40keV			
Horizontal aperture (μrad)	*Beam size at sample (mm)*	*H divergence (μrad)*	*V divergence (μrad)*
300	*2.9*	*273*	*4.1*
400	*3.8*	*363*	*4.5*
600	*5.5*	*542*	*5.0*
1000	*7.1*	*596*	*5.5*

As can be seen from table 4.11 the horizontal focusing slightly deteriorates the divergence in the vertical plane (and introduces asymmetry). The influence can be reduced by closing the horizontal slits. The energy resolution is not affected.

Spot shape and divergences at the PD sample position for the following case:

Horizontal divergence accepted into the BL: 1000µrad

Horizontal divergence allowed to the sample is set by a slit 1m before M2

K: 3.65, 30keV, R_s=5cm, R_M=∞ (cylinder mirror)
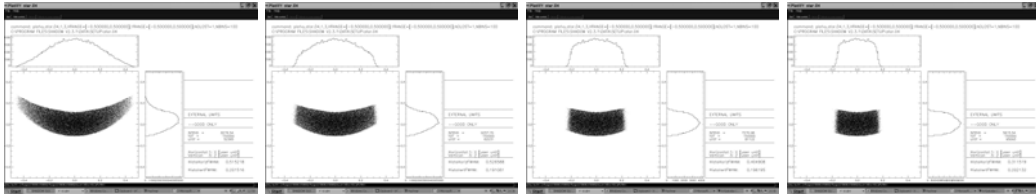
Figure 4.8: Spot in horizontal (X) and vertical (Y) direction at different horizontal acceptances (1000, 600, 400, 300µrad), equal scaling X, Y.
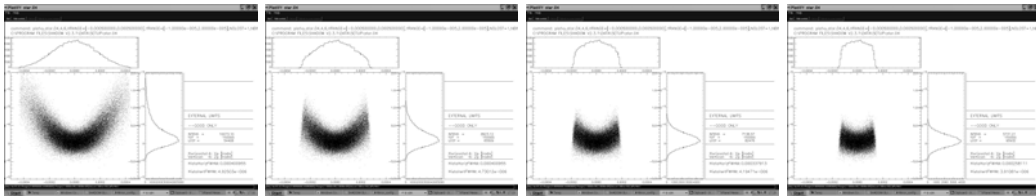
Figure 4.9: Divergence in the horizontal (H_{Div}) and vertical (V_{Div}) direction at different horizontal acceptances (1000, 600, 400, 300µrad). Scale: H_{Div}+- 500µrad, V_{Div} -10/+20µrad
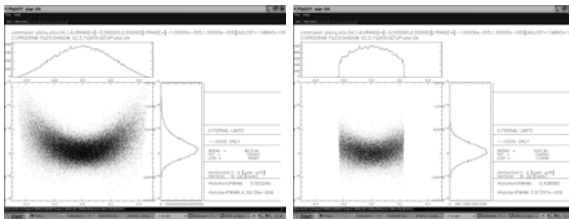
Figure 4.10: Vertical divergence V_{Div} versus horizontal position X with 1000µrad and 600µrad of the beam horizontally accepted by the BL. By reducing the horizontal slit size (upstream M1) the vertical divergence can be reduced and the distribution becomes more symmetric.
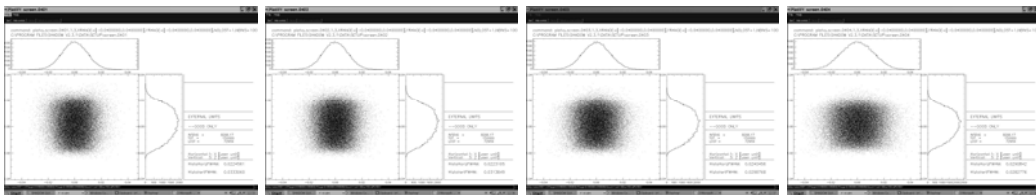
Figure 4.11: SC station out of focus with: K=3.65, θ_{M2}=3.1mrad, $R_{meridional}$=9km, $R_{sagittal}$=5cm, 20keV, distances: 35.9 / 36 / 36.1 / 36.2m, same scaling in X and Y direction, Spot size HxV: 0.22 x 0.31mm^2.
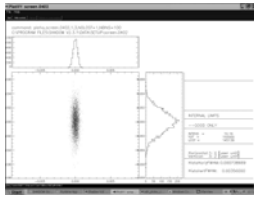
Figure 4.12: KB spot size. The diagram is 90° rotated. Values for the calculation are given in section 4.2.7.

Size H x V: 36 x 7μm

Divergence H x V: 1100 x 930μrad

4.3 Heat load effects on optical elements, slope errors

The FEA calculations for the temperature distribution and deformations on the mirror and monochromator crystal were performed by M. Quispe and L. Nikitina from ALBA with the program packages ANSYS and ANSYS workbench.

In section 4.1 the total absorbed heat loads for different operational conditions are given. One design criterion for the beam line optics is the maximum absorbed power in the first pre-filter, thus defining the maximum aperture. At 400mA ring current and 1000μrad horizontal acceptance the absorbed power in this first filter is already too high, at the nominal current of 250mA it is at the limit (550W, 592W for K6.08 and 3.65 and 0.3mm absorber thickness). A horizontal acceptance below this value is therefore more likely and 600μrad is taken as typical. As the low energy region is not the focus of this beam line the power on the optics can be adapted by low-Z absorbers with variable thickness and in the energy regime of 8-20keV also by reducing the wiggler K-value. To investigate the heat load effects especially the high energy regime with maximum K-value was considered. As maximum acceptable power load on the monochromator a value of about 650W was assumed and the filters adjusted correspondingly. This filter setting was then also used for lower photon energies. A power load of about 870W in the Si-stripe and 270W in the Pt-stripe of the mirror and correspondingly 70W and 670W in the first monochromator crystal was calculated (10keV and 40keV).

4.3.1 Heat load on collimating mirror

Si coating

The Si coated mirror stripe absorbs about three times more heat than the Pt stripe. Although the collimation requirements are more relaxed in the low energy region, this is assumed as a worst case.

The values for calculation are:

K=6.08, 400mA Synchrotron current,

Aperture HxV: 600x125μrad^2

Filter: 9.3mm Pyrographite, 0.3mm Be

Mirror angle: 2mrad

Total absorbed power: 872W

Peak power density: 0.0693W/mm^2

Thermal conductivity of contact material Galinstan: 16.5 W/m°C

Mirror geometry is given in 4.2.4
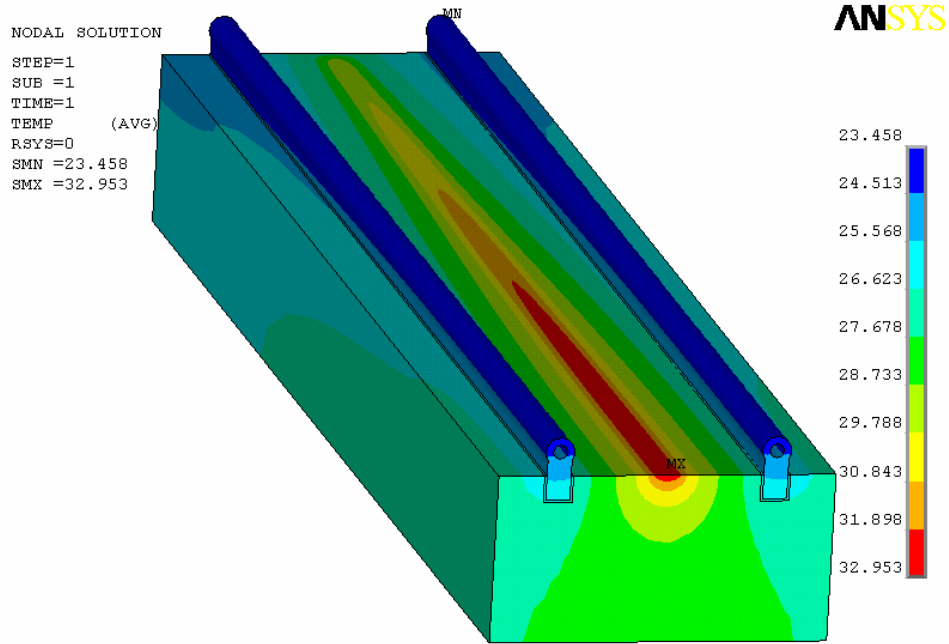
Figure 4.13: Temperature distribution on the mirror.
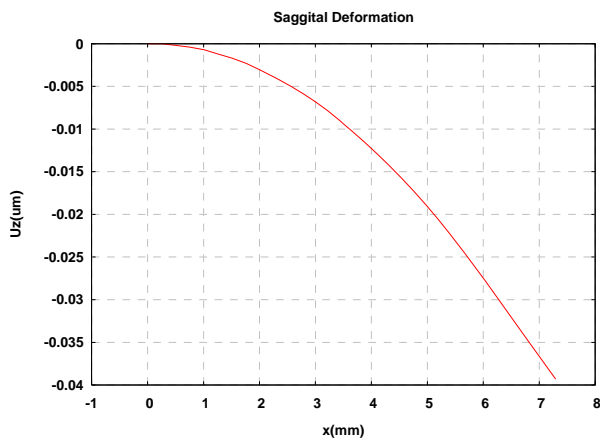
Figure 4.14: Sagittal deformation profile.
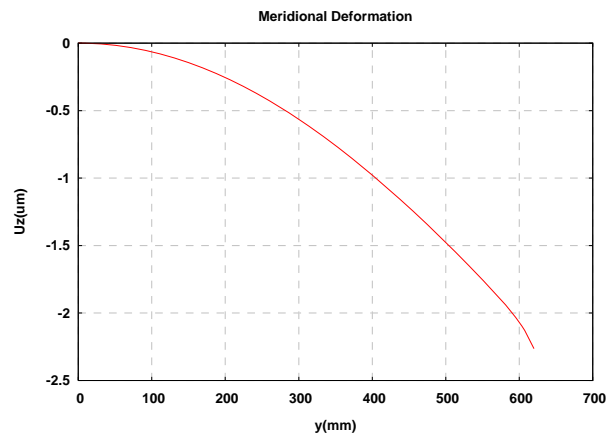
Figure 4.15: Meridional deformation.

Ray-tracing:

Residual divergence with $R_{meridional}$ =20km (M1): V_{Div}= 23.3µrad. (K 6.08, 10keV)

Residual divergence with $R_{meridional}$ =16.5km (M1): V_{Div}= 7.2µrad. (K 6.08, 10keV)

The effects of 872W absorbed power can mostly be compensated by changing the curvature of M1 to 16.5km.

4.3.2 Heat load on CCM

Two cases of absorbed power on the monochromator for 40keV and 20keV are presented:

I) 40keV

Values used for calculation:

K=6.08, 400mA Synchrotron current,

Aperture H x V:	600x125µrad^2,
Filter:	9.3mm pyrographite, 0.3mm Be
Crystal dimensions W x L x H:	50x93x55mm^3
Footprint on surface H x V:	13.4 x 50mm^2
Energy:	40keV
Total absorbed power:	668W
Peak power density:	1.15W/mm^2
Coolant temperature:	77K
Thermal conductance coefficient Cu/Si:	6000W/m^{2}K
Convective heat transfer coefficient (lN2):	6000W/m^{2}K
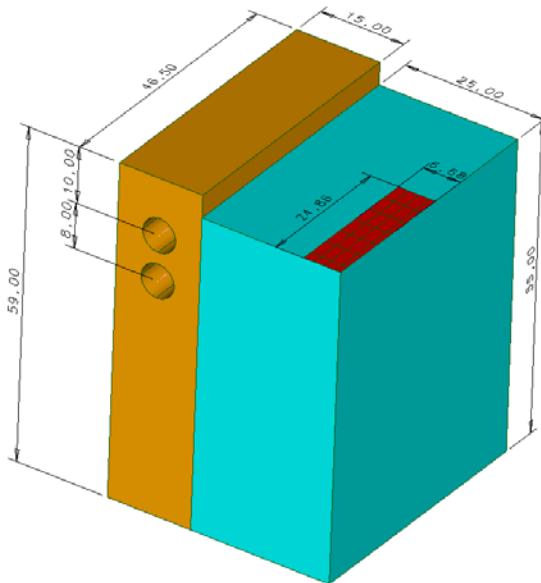
Figure 4.16: Quadrant of the Monochromator crystal used for FEA calculations (40keV case).
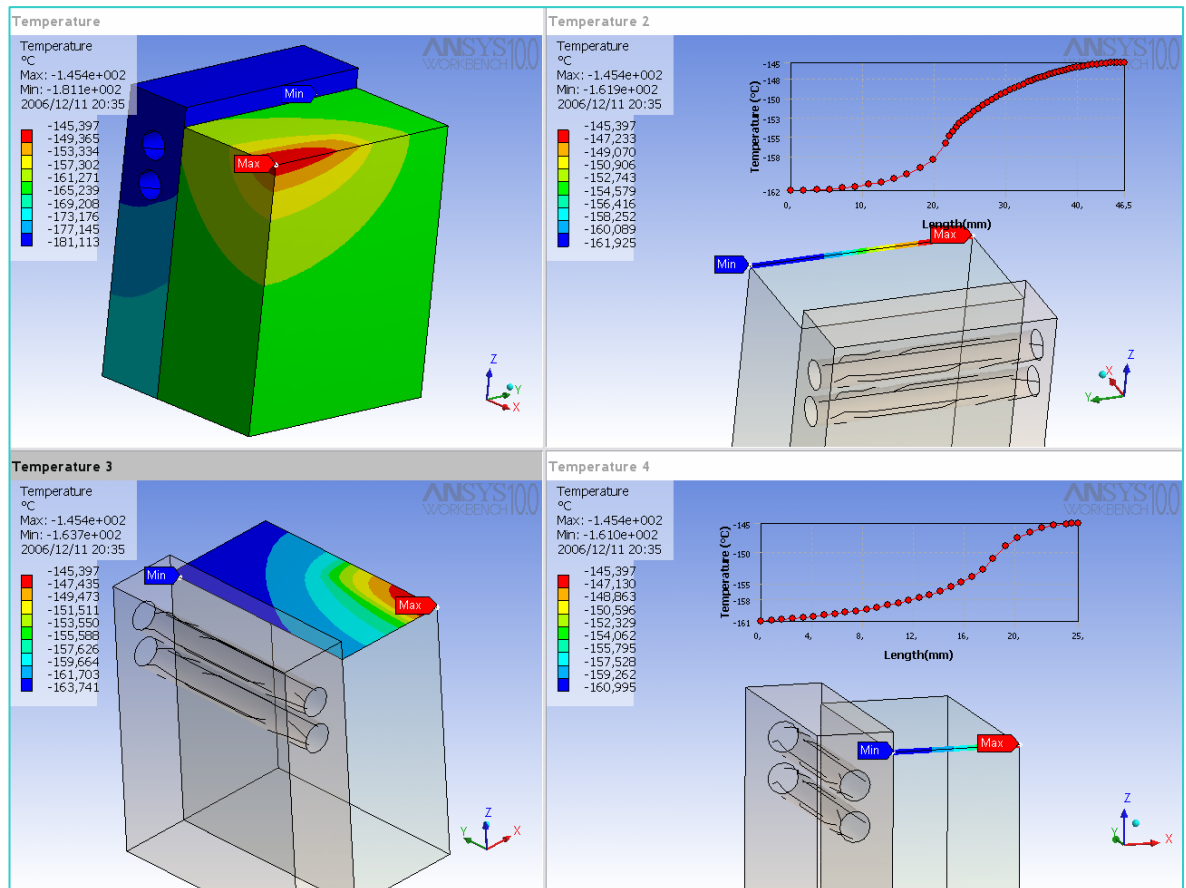
Figure 4.17: Temperature distribution on the monochromator crystal, 40keV case.

Maximum temperature in the hot spot: 127.6K

Maximum temperature difference in the footprint is about 13K

Assuming a thermal expansion coefficient of $1.4 \cdot 10^{-7}$ at 115K this leads to a strain of $dD/D = 1.9 \cdot 10^{-6}$.

A value of 6000W/m^{2}K for the heat transfer coefficient between Si and Cu is typically used for calculations. If the thermal contact is worse, the temperature in the hot spot rises:

Heat transfer coefficient	$T_{hot\ spot}$
6000W/m^{2}K	128K
4000W/m^{2}K	136K
2000W/m^{2}K	160K

The effect of surface deformation on the first monochromator crystal was estimated with ray-tracing calculations using the z-deformation from FEA calculations (figure 4.18).
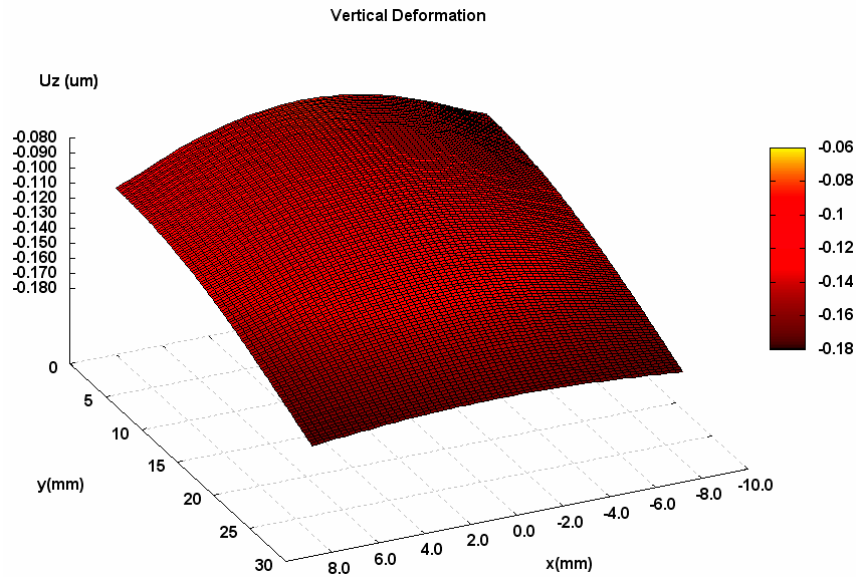
Figure 4.18: Deformation in z-direction at 40keV with values given in the text.

	R$_M$ [km]	V$_{Div}$ [μrad] after Mono	V$_{Div}$ [μrad] @ sample	dE [eV]	dE/E	Efficiency T (see 4.2.8)
No heat	100	3.9	17	5.4	1.4e-4	.24
668W abs.	100	16.5	5	9.6	2.4e-4	.11
No heat	30	3.9	60	5.4	1.4e-4	.24
668W abs.	30	16.5	46	9.6	2.4e-4	.11

Table 4.12: Effect of the thermal bump on the first monochromator crystal at 40keV (assuming an ideal collimating mirror M1) and with M2 bent to 30km.

There is a considerable loss in energy resolution at 40keV with 668W absorbed power. But since this setup is mainly dedicated to high pressure and total scattering experiments it is acceptable. Ray-tracing shows also a decrease in transmitting efficiency due to the bump of about 50%. The additional divergence from the heat bump can partly be compensated by changing the meridional curvature (collimation) of M2 (see table 4.12).

I) 20keV

The same situation as before, with Pt-collimating mirror exchanged by Rh-mirror and energy set to 20keV:

Total absorbed power: 527W

Peak power density: 1.78W/mm^2

Footprint W x L: 13.4 x 25mm^2

Vertical Deformation
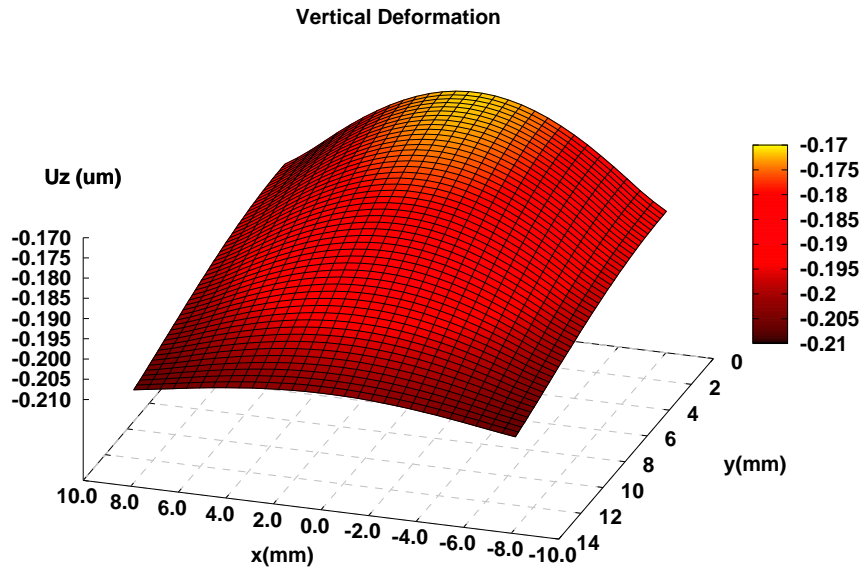
Figure 4.19: Deformation in z-direction at 20keV with values given in the text.

	V_{Div} [µrad] after Mono	dE [eV]	dE/E
No heat	6.2	2.7	1.35e-4
527W abs.	12.7	2.8	1.4e-4

Table 4.13: Effect of thermal bump on first monochromator crystal at 20keV (assuming an ideal collimating mirror M1).

The increase in vertical divergence as well as energy resolution is acceptable with 572W absorbed power. Ray-tracing calculations show a decrease in transmitting efficiency of the order of 10-15%.

Mirror slope error:

Polishing sometimes introduces waviness with certain period length like ~150mm [Patterson05]. Although the influence of slope error on the optical performance strongly depends on the actual power spectral density (PSD) of the slope, a wavy surface was modeled to estimate the effects. The surface was generated with the shadow tool waviness_gen.exe with an input rms slope error of 0.5arcsec (~2.5µrad) and up to 8 harmonics. The surface is shown in figure 4.20. The distortion led to an increased vertical divergence of 5.1µrad FWHM (ideal 3.9µrad) and a transmitted energy band of 5.6eV @40keV (ideal 5.4eV) at a radius of curvature of 20km and 2mrad glancing angle.

Since mirrors of 1200mm length can nowadays be manufactured with 1.5µrad slope error and better, the 2.5µrad for the calculation can be considered as an upper limit.

More critical is the intensity structure generated in the beam when working out of focus, like at the PD station in the collimated beam. Therefore, and also considering a large radius of curvature (20km), the slope errors should be as small as possible (1µrad).
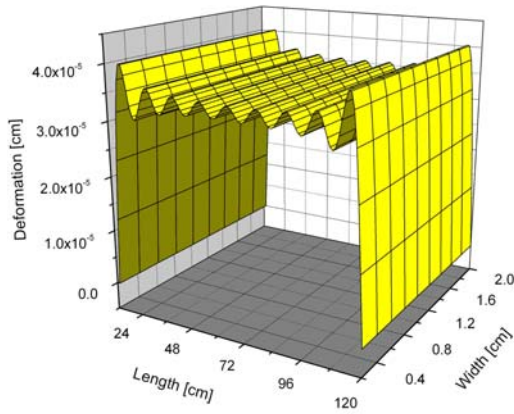
Figure 4.20: Simulated surface deformation for 2.5µrad rms-slope error.

Table 4.14: Vertical divergence and transmitted energy band with ideal and deformed M1 surface. K=6.08

	V_{div} [µrad]	dE
10keV	7.3	1.3 (ideal)
	8.3	1.3 (2.5µrad slope error)
20keV	5.3	2.7 (ideal)
	63	2.7 (2.5µrad slope error)
40keV	3.9	5.4 (ideal)
	5.0	5.6 (2.5µrad slope error)
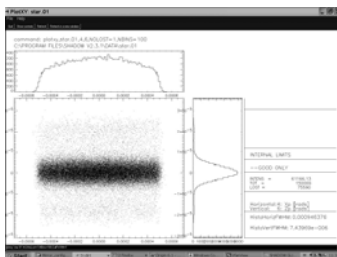
Figure 4.21: Vertical divergence after collimating mirror with slope error from figure 4.20 (2.5µrad rms-slope error).
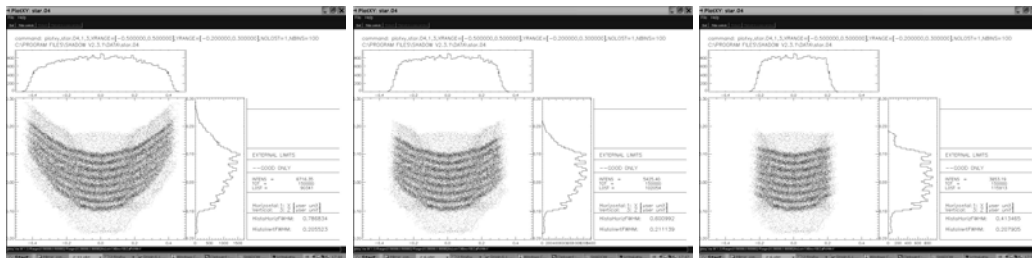
4.22: Spot size at PD station with the same surface error for M1 and M2 for 1000µrad, 600µrad and 400µrad horizontal aperture. The wavy structure is due to the purely periodic type of slope error assumed.

H-aperture	1000 [μrad]	600 [μrad]	400 [μrad]
V_{Div} [μrad]	11.0	9.8	9.1
H_{Div} [μrad]	650	519	343
V_{size} [mm]	2.1	2.1	2.1
H_{size} [mm]	7.9	6.0	4.1

Table 4.15: FWHM values for spot size and divergence with slope error on M1 and M2 given in the text.

Figure 4.23 gives the spot size at the PD station in a focusing condition. The values are set to illuminate a typically sized sample. The resulting vertical divergence of M2 is used in section 4.4 to calculate the instrumental resolution function.
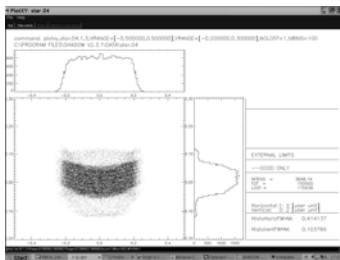
Figure 4.23: Spot size with meridional focusing (R=30km) of M2: HxV: $4.1 \times 1.0 \text{mm}^2$.

4.4 Effect of the focusing second mirror on the instrumental resolution function

Mirror M2 transfers horizontal divergence into the vertical diffraction plane already without bending. This influences width and shape of the powder reflection profiles. With reduced horizontal aperture (<600μrad) the angular distribution in the vertical plane can be kept considerably symmetric and small (and therefore the reflection profiles). Figure 4.24 shows the instrumental resolution function IRF at 20keV according to Eq. 4.2 assuming an ideal collimating mirror (R_M=20km) with V_{Div}=5.2μrad, and a corresponding vertical divergence for a flat (V_{Div}=7μrad, R_S=5cm) and bent (V_{Div}=64.5μrad, R_M=30km, R_S=5cm) M2 from ray-tracing. Since the ray tracing program can not handle toroidal mirrors with infinite R_M in some calculations a value of R_M=100km was assumed. The calculations differ slightly compared to a purely sagittally curved cylinder mirror. The vertical divergence at the sample position assuming a toroidal mirror (approximating a flat mirror) with R_M=100km is at all energies about V_{Div} = 17.5μrad.

$\Delta\tau_p$ = 5.2μrad

Δ_m = Δ_a = 14μrad

θ_m = θ_a = 4.12°
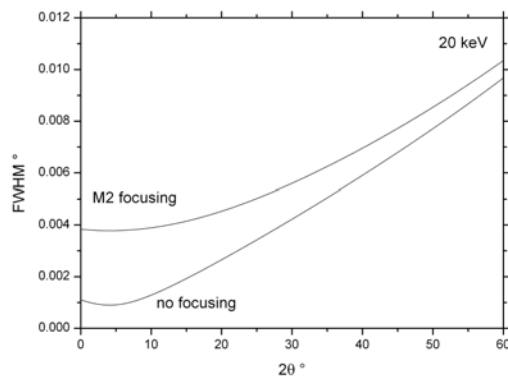
$\Delta\tau_f$ = 7μrad and 64.5μrad

Figure 4.24: IRF at PD with and without bent M2 (see text).

4.5 Misalignment of M2

The probably largest influence on the optical performance has a misalignment of M2. Therefore, several cases were investigated with ray-tracing. A degree of freedom for the alignment of the mentioned axes is necessary.

- Height: due to the non constant beam offset from the CCM a change in height of about 0.2mm is possible. Calculations show that changes in beam size and divergence are of the order of 10% or less and their distributions are similar to the ideal case. Beside realignment of the sample height this doesn't implicate serious problems.

- Lateral shift: A lateral shift of 1mm was assumed for ray-tracing calculations. They show a non acceptable deviation from the ideal case and the alignment has to be considerably better.
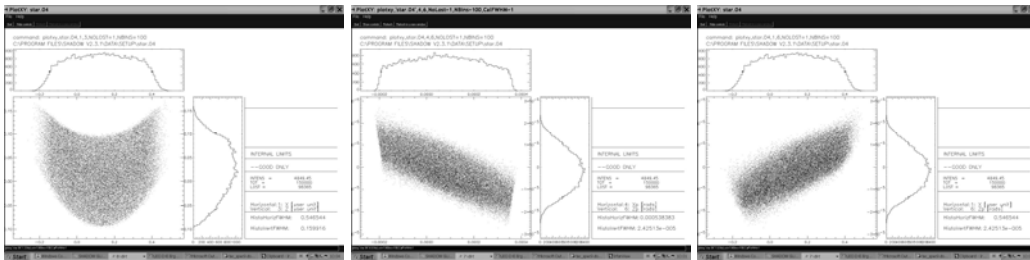
Figure 4.25: Deviations at the PD station from a 1mm lateral misalignment of M2. The center of the spot is shifted by more than 1mm. From left to right: Position, V vs. H Divergence, V_{Div} vs. horizontal position.

- Rotation around vertical axis (yaw): A rotation around the vertical axis of 1mrad show effects analog to the before mentioned case.
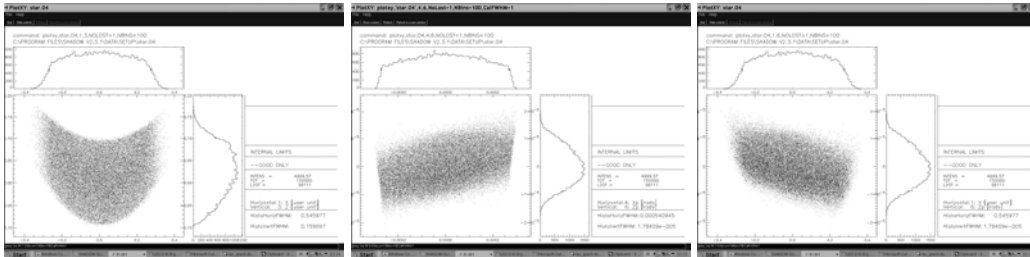
Figure 4.26: Deviations at the PD station from a 1mrad rotation of M2. The center of the spot is not shifted. From left to right: V vs. H Position, V vs. H Divergence, V_{Div} vs. horizontal position.

- Lateral shift plus rotation: Both movements are not completely independent and can partly be compensated by each other. Figure 4.27 shows the effect at the PD station with 0.5mm lateral shift and 1mrad rotation around the vertical axis.
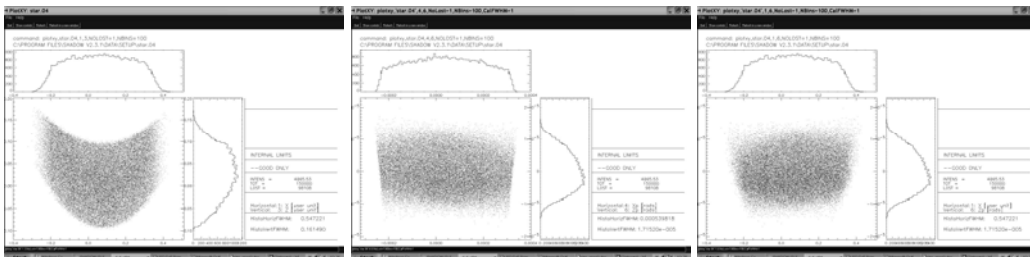
Figure 4.27: Deviations at the PD station from a 0.5mm lateral shift and 1mrad rotation around vertical axis of M2. The center of the spot is shifted by about 0.8mm. From left to right: Position, V vs. H Divergence, V_{Div} vs. horizontal position.

5   Beam shaping and diagnostics

Beam shaping

The maximum beam allowed into the beam line is defined by the fixed aperture in the FE to 1.5x0.25mrad. A so called movable absorber in the front end acts as white beam slit and defines the beam size allowed on the optics. This device consists of inclined water cooled Glidcop blades with tungsten edges on the downstream side.

If possible (concerning space in the optics hutch) a second white beam slit should be installed in the optics hutch between first mirror and CCM. The first absorber will only be moved during the initial alignment and afterwards decoupled. The beam size can then be defined by the second slit from the user, thus reducing the risk of damaging the optics by unintended opening of the slit. Additionally, a white beam slit is needed when the beam line is operated at high energies without the first mirror. Monochromatic beam slits will be inserted downstream the CCM and downstream the second mirror.

Additional slits/collimators at the SC/HP station and in the KB-mirror system are not considered here.

Beam diagnostics

Ideally one should be able to monitor the beam before and after each optical element, preferably intensity, position and beam shape. The first XBPM is located in the FE region to control the orbit of storage ring. This signal will also be used for the BL. In addition we plan to install XBPM/I0 monitors just after M1, CCM and M2. These monitors should be adaptable to the beam offsets along the optics (see section 7). The specific monitor types are not yet definitely decided. For initial alignment of the CCM the W-collimator should be moved downwards so that the direct beam can be seen from a downstream monitor. Other alignment tool is an optical camera with fluorescent screen and high resolution located at the experimental stations.

Conventional ionization chambers or scattering foil/pin diode detectors to measure intensity and polarization will be placed along the beam line downstream M2.

6   Experimental stations and detectors

The beam line will be host for a wide range of experiments with different needs, thus sample environment and detectors should show some flexibility for the application at both experimental stations, if possible.

The number and type of detectors is not yet finally decided. However, the following considerations should be taken into account.

- HP diffraction needs an image plate detector. The aperture of the DAC is typically below 60º and the whole diffraction cone should be recorded at once. Image plates have large apertures, high dynamic range and low intrinsic noise at long exposures. .
- SC measurements need a fast readout area detector: CCD.
- Both the SC/HP station should have a point detector. Point detectors can be used together with collimators to reduce the scattered background from e.g. DACs.

- The main detector for the high resolution powder diffraction station will be a multi analyzer stage with 5-7 detectors + analyzer crystals (Si111, Ge111 or ML) on an exchangeable mounting plate (see figure 6.1). For experiments not requiring maximum energy resolution ML mirrors are planned to be used. Multilayers with low contrast and low-Z materials and about 100 double layer periods can nowadays reliably be manufactured. Those analyzers seem to be ideal for applications needing intermediate resolution of about $2 \cdot 10^{-3}$ like total scattering experiments at energies between 30-50keV. Stacks of parallel foils ("Soller-Slits") should also be considered.

- Time resolved PD experiments can be performed on very different time scales. In the minutes range the multidetector, as well as a curved 1-dim PSD are adequate. To perform for instance stroboscopic measurements a PSD is necessary. Below one second time resolution the curved silicon strip detector developed at the Swiss Light Source (Mythen-detector) is feasible. For the beginning it is planned to use the CCD detector from the SC station, either as area detector or, with a suitable mask in front, in a "shift-register"-like mode. A high data quality from the detectors should always be considered.

Station 1:

The SC station needs a Kappa or a four circle diffractometer, while for HP applications a two circle diffractometer (ω and χ) with additional sample translation stage for micro positioning is required. It's necessary to find a diffractometer that accommodates both techniques without major changes in the hardware. It's also important to have enough free space around the diffractometer to install additional equipment like lasers and other sample environments. Diffractometer, KB-mirror and both Laser systems will be installed on a common 2 x 3m granite slab.

Station 2:

The PD station should mainly consist of three concentric rotary tables with angular resolution of about $1 \cdot 10^{-4}$ deg. This way it's possible to install both, PSD and Multidetector at the same time. Opposite to the diffractometer an additional independent and adjustable table should be available to carry large and heavy sample environments. Figure 6.2 shows a drawing of the diffractometer used at the MS beam line at the SLS.
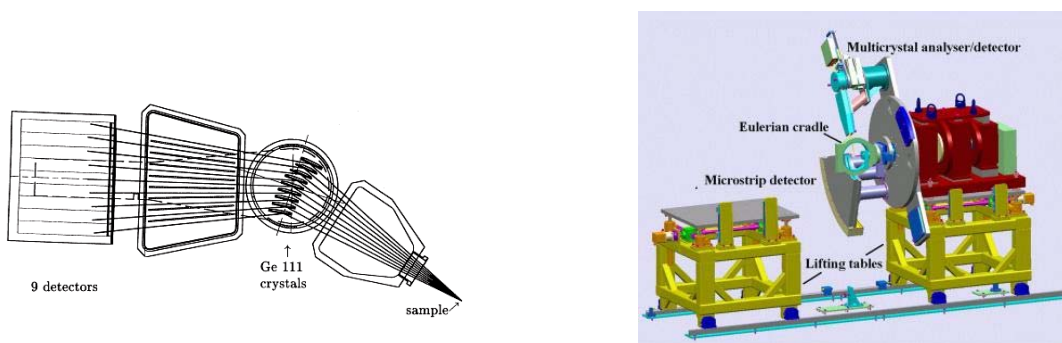
Figure 6.1: Left, multianalyzer detector for high resolution powder diffraction (Hodeau98).

Figure 6.2: Right: SLS Diffractometer, it provides excellent resolution, and both flexible detector system and sample environment installation.

Lateral space to neighboring BL:

The option to install a beam line at the downstream (neighboring) bending magnet port should be kept open. This beam line is then directly next to the MSPD with its source point shifted by about 4.3m downstream the ring and a take off angle of 4.63°. This results at the two experimental stations in a beam separation of:

Station 1 @ 36m: 2.5m

Station 2 @ 39m: 2.8m

The final layout of the experimental stations will be worked out during summer 2007.

7   Beam line components layout

7.1 Positions along the beam

Positions along the beam (total maximum length 42 m)

Vacuum section 1

*Elements→*FE Gate valve→Filter 1→Filter 2→Be vacuum window →White beam filter→Valve→

                                C0.3   C1   Be0.3   C0-C8

Positions: 18.2 m

Pipe diameter 40 mm

fixed height (0 mm with respect to the orbit)

Vacuum section 1.1

Elements: M1 collimating mirror

Positions: 20 m

Vacuum section 2

Elements: Valve (White beam slit) →XBPM/I0→Valve

Pipe diameter: 60 mm

fixed height: 0 mm

Vacuum section 2.1

Elements: flexible bellow→CCM→W collimator 200 mm→flexible bellow

Positions: 22 m

(*) flexible: bellow 150 mm

Height min. (no mirror): 8 mm

Height max. (mirror): 26 mm

Vacuum section 3

Elements: valve →Monochromatic beam slit →XBPM/I0 monitor→valve

Pipe diameter: 60 mm

Height min. (no mirror): 8 mm

Height max. (mirror): 26 mm

Vacuum section 3.1

Elements: flexible bellow →M2 sagittally focusing mirror →flexible bellow

Positions: 24 m

Vacuum section 4

Elements:Valve → Monochromatic beam slit → Monochromatic beam filter → Fast shutter → I0 monitor → Photon beam shutter → Optics hutch wall

Positions: 28 m

Pipe diameter: 60 mm

Height min. (no mirror): 8 mm

Height max. (mirror): 44 mm

In vacuum section 3 and 4 all components are mounted on a common girder. This girder is movable in height for about 30mm (VS 3) and 50mm (VS 4). All components on the girder can thus be translated vertically for the mirrored and un-mirrored setup.
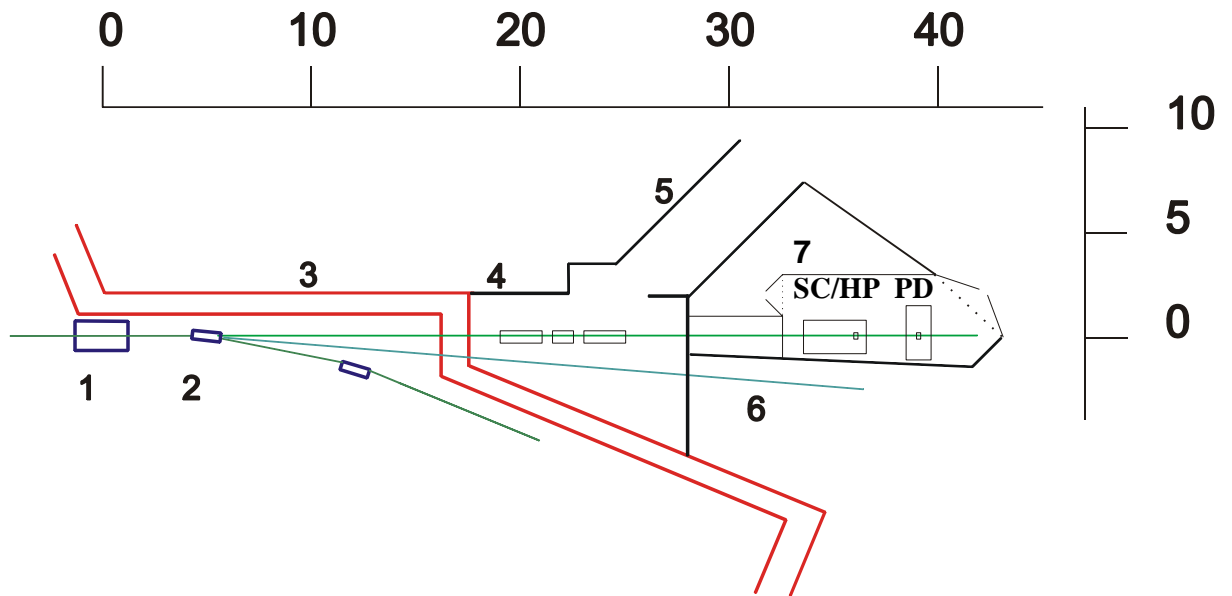
Figure 7.1: Preliminary layout of the hutches, distances given in meters. 1: ID, 2: next bending magnet, 3: shield wall, 4: optics hutch, 5: access to optics hutch, 6: neighboring beam line, 7: experimental hutch.

7.2 Beam offsets

In table 7.1 the values for the offsets in beam height are given for the different optical configurations.

Table 7.1: Maximum beam offsets from orbital height (1400mm) for a mono gap of 4mm. The values are given for two different mirror angles (2mrad, 3mrad) and three distances between M1-CCM-M2 (2m, 2.5m, 3m).

M1-CCM(=CCM-M2) distance Mirror angle	Before 1st mirror	At CCM	After CCM	At M2/sample
2 m 0mrad	0	0	8	8
2 m	0	8	16	24

2mrad				
2 m 3mrad	0	12	20	32
2.5 m 2mrad	0	10	18	28
2.5 m 3mrad	0	15	23	38
3 m 2mrad	0	12	20	32
3 m 3mrad	0	18	26	44

8 Other design concepts

8.1 M2: double toroidal mirror

An alternative to M2 is the use of two Pt-coated cylinder mirrors next to each other, either on a common mirror or on two mirrors with a common bender and lateral translation. The additional mirror has a smaller radius of curvature of about 32 mm giving the opportunity of focusing on the HP station at a mirror angle of 2mrad and therefore operating up to 40keV. The polishing of two different diameters on one mirror body includes the risk of damaging the first surface while polishing the second. The option of two mirrors with the corresponding mechanics in one vessel increases the cost considerably. The gain in performance by having this focusing option on station 1 up to 40keV is maybe not sufficient and a multilayer device for the energy range above 40keV is still necessary. Particularly as this multilayer KB optics can also be used in the energy range below 40keV. Therefore, this option should not be considered.

8.2 Reduced sagittal radius for M2

In case of using a mirror with only one sagittal curvature, the radius could be reduced to 40mm enabling a glancing angle of 2.5mrad while focusing on station 1 and thereby increasing the available energy range to above 30keV. This energy is reasonable for performing high pressure experiments on station 1. But this radius already introduces a considerable divergence in the vertical plane on the PD station when used a 2mrad, as well as a very small horizontal beam dimension. This disadvantage doesn't justify the smaller radius.

8.3 CVD Diamond filter

Using CVD diamond windows as a combined filter/vacuum window is an option more widely used at ESRF undulator beam lines. The accepted heat loads are comparable to a conventional graphite filter / Be-window combination, at least for windows with rather small apertures. The performance of windows with rather big apertures (up to 20 mm) is not yet well investigated. Besides, the cost is considerably higher. The improvement in

beam quality due to reduced scattering in the window is no real advantage, since the source size is rather large and additional filters have to be used in many cases.

8.4 Additional White beam slit

An additional white beam slit between collimating mirror M1 and monochromator enables adaption of the beam size without touching the movable absorbers in the FE region. It's also useful for defining the beam size on the monochromator in the un-mirrored mode. Since the distance between the centers of M1 and CCM is only 2m for an exact 2:1 focusing condition (otherwise the distance between the two stations gets to small) it's difficult to fit it in the beam path. It might be possible to find a compromise in the layout and therefore some space to fit it in.

8.5 DCM with sagittally curved second crystal

This is a widely used concept: The second crystal consists of a thin plate with ribs on the back side. A bender can give a sagittal curvature and focus to the desired position. Disadvantages from this design are

- difficulties in cryo-cooling the second crystal.

- not decoupled focusing/monochromatization.

- residual structure in the flat crystal plate resulting from the ribs.

- anticlastic bending changes longitudinal slope and reduces transmitted intensity.

8.6 Compound refractive lenses CRL

CRLs consist of a stack of spherical or parabolic low-Z concave lenses and work very efficiently at high energies [Elleaume98]. Due to le low index of refraction for X-rays dozens to hundreds of single lenses have to be arranged in one stack to get a reasonable short focal length. From their optical requirements they are less sensitive to surface roughness, compared to mirrors; they're also relatively easy to align and cheap. Radius of curvature, energy of the radiation, lens material and focal length are related to transmittance and useful aperture. The expected aperture is about 1mm or below. Some space is reserved in the optics hutch downstream M2 to include CRLs later.

9 References

A detailed description of the scientific case can be obtained from the original proposal

http://www.cells.es/static/Powder_and_High_Press_Diff.pdf

R. Caciuffo, S. Melone, F. Rusticelli. *Monochromators for X-ray synchrotron radiation.* Phys. Rep. 152 (1987) 1-71.

J. Campmany. *Conceptual Design of a Superconducting wiggler for the Powder Diffraction beamline.* Internal report AAS-SR-ID-AN-0121 (2006).

J. Campmany. *Parameter optimization of a wiggler for feeding the Powder Diffraction Beamline at ALBA.* Internal report AAS-SR-ID-AN-0140 (2006).

J. Campmany. *Ripple in the spectrum at high energies for SC-W31 wiggler. ADDENDUM to Conceptual Design of a Superconducting wiggler for the Powder Diffraction beamline, document AAS-SR-ID-AN-0121 (2007).*

O. Chubar, P. Elleaume, J. Chavanne, *A 3D Magnetostatics Computer Code for Insertion devices*, J. Synchrotron Rad. 5 (1998), 481-484.

A. Chumakov, R. Rueffer, O. Leupold, J. P. Celse, K. Martel, M. Rossat, W. K. Lee. *Performance of a cryogenic silicon monochromator under extreme heat load.* J. Synchrotron Rad. 11 (2004) 132-141.

P. Elleaume. *Optimization of compound refractive lenses for X-rays.* NIM A 412 (1998) 483-506.

J. I. Espeso, P. Cloetens, J. Baruchel, J.Haertwig, T. Mairs, J. C. Biasci, G. Marot, M. Salome-Pateyron, M. Schlenker. *Conserving the Coherence and Uniformity of Third-Generation Synchrotron Radiation Beams: the Case of ID19, a `Long' Beamline at the ESRF.* J. Synchrotron Rad. 5 (1998) 1243-1249.

F. Gozzo, L. De Caro, C. Giannini, A. Guagliardi, B. Schmitt, A. Prodi. *The instrumental resolution function of synchrotron radiation powder diffractometers in the presence of focusing optics.* J. Appl. Cryst., 39 (2006) 347-357.

J. L. Hodeau, P. Bordet, M. Anne, A. Prat, A. N. Fitch, E. Dooryhee, G. Vaughan, A. Freund. *Nine crystal multi-analyzer stage for high resolution powder diffraction between 6 and 40keV.* SPIE proceedings Vol. 3448 (1998) 353-361.

O. Masson, E. Dooryhee, A. N. Fitch. *Instrument line-profile synthesis in high-resolution synchrotron powder diffraction.* J. Appl. Cryst. 36 (2003) 286-294.

B. D. Patterson, R. Abela, H. Auderset, Q. Chen, F. Fauth, F. Gozzo, G. Ingold, H. Kuehne, M. Lange, D. Maden, D. Meister, P. Pattison, Th. Schmitt, B. Schmitt, C. Schulze-Briese, M. Shi, M. Stampanoni, P. R. Willmott. *The materials science beamline at the Swiss Light source: design and realization.* NIM A 540 (2005) 42-67.

M. Sanchez del Rio, R. J. Dejus. *XOP: A Multiplatform Graphical User Interface for Synchrotron Radiation Spectral and Optics Calculations.* SPIE Proc., 3152 (1997) 148.

G. Tajiri, W. K. Lee, P. Fernandez, D. Mills, L. Assoufid, F. Amirouche. *Nonlinear thermal-distortion predictions of a silicon monochromator using the finite element method.* J. Synchrotron Rad. 8 (2001) 1140-1148.

T. Tanaka and H. Kitamura. *SPECTRA: a synchrotron radiation calculation code.* J. Synchrotron Rad. 8 (2001) 1221-1228.

L. Zhang, W. K. Lee, M. Wulff, L. Eybert. *The performance of a cryogenically cooled monochromator for an in-vacuum undulator beamline.* J. Synchrotron Rad. 10 (2003) 313-310.

10 Appendix

Total flux of ID attenuated corresponding to a specific horizontal aperture:

K 6.08, I=400mA	C5.3,Be0.3 (400μrad)	C9.3,Be0.3 (600μrad)	/
10keV	2.65e14	3.19e13	/
20keV	1.28e15	8.57e14	/
30keV	7.40e14	5.87e14	/
40keV	3.59e14	2.98e14	/
K3.65, I=400mA	C1.3Be0.3 (400μrad)	C2.3Be0.3 (600μrad)	/
10keV	8.17e14	4.81e14	/
20keV	4.07e14	3.69e14	/
30keV	1.17e14	1.1e14	/
40keV	3.18e13	3.03e13	/
K6.08, I=250mA	/	C5.3Be0.3 (600μrad)	C9.3Be03(1000μrad)
10keV	/	1.66e14	1.91e13
20keV	/	7.98e14	5.36e14
30keV	/	4.62e14	3.67e14
40keV	/	2.24e14	1.86e14
K3.65, I=250mA	/	C1.3Be0.3 (600μrad)	/
10keV	/	5.1e14	/
20keV	/	2.55e14	/
30keV	/	7.29e13	/
40keV	/	1.99e13	/